Literature Study Hopper Loading

OE44140 Multidisciplinary Project

B.F. Sloof - 4158768

Delft University of Technology

TU Delft Delft University of Technology

DAMEN

Contents

Nomenclature

Greek Symbols

α	Concentration	$[-]$
α_b	Near bed concentration	$[-]$
α_k	Concentration of fraction k	$[-]$
α_{bed}	Concentration in the bed cell	$[-]$
α_{liquid}	Concentration in the cell above the bed	$[-]$
α_{merged}	Concentration in the cell after merging	$[-]$
β	Slope angle	$[^\circ]$
Δ	Specific sediment density	$[-]$
$\dot{\gamma}$	Shear rate	$[1/s]$
ϵ	Dissipation of turbulent kinetic energy	$[J/(kg \cdot s)]$
Γ	Diffusion coefficient	$[m^2/s]$
κ	Von Karman constant	$[-]$
μ	Dynamic viscosity	$[Pa \cdot s]$
μ_{eff}	Effective viscosity (dynamic)	$[Pa \cdot s]$
ν	Kinematic viscosity	$[m^2/s]$
ν_e	Eddy viscosity (kinematic)	$[m^2/s]$
ν_m	Molecular viscosity (kinematic)	$[m^2/s]$
ν_{eff}	Effective viscosity: summation of eddy and molecular viscosity	$[m^2/s]$
ω	The specific turbulence dissipation rate	$[1/s]$
Φ	Pickup flux	$[-]$
ϕ	Angle of internal friction	$[^\circ]$
ϕ	Volume flux through a face	$[m^3/s]$
Ψ	Shape factor	$[-]$
ρ	Density	$[kg/m^3]$
ρ_k	Density of fraction k	$[kg/m^3]$
ρ_m	Mixture density	$[kg/m^3]$
ρ_s	Solids density	$[kg/m^3]$
ρ_w	Water density	$[kg/m^3]$
σ	Schmidt number	$[Pa]$
τ	Shear stress	$[Pa]$
τ_y	Yield stress	$[Pa]$
θ	Shields number	$[-]$

θ_{cr}	Critical shields number	$[-]$
θ'_{cr}	Critical shields number adjusted for high speed and slope	$[-]$

Roman Symbols

$\mathbf{j}_m$	Mixture flux velocity vector	$[m/s]$
$\mathbf{S}_f$	Surface vector of a face	$[m^2]$
$\mathbf{T}_m$	Viscous stress tensor	$[Pa]$
$\mathbf{T}_m^t$	Turbulent stress tensor	$[Pa]$
$\mathbf{u}$	Velocity vector	$[m/s]$
$\mathbf{u}_k$	Velocity vector of fraction k	$[m/s]$
$\mathbf{u}_m$	Mixture centre of mass velocity vector	$[m/s]$
$\mathbf{u}_{kr}$	Slip velocity vector of fraction k	$[m/s]$
C	Constant for rough wall function	$[-]$
C_D	Drag coefficient	$[-]$
c_k	Mass fraction of k	$[m]$
D	Particle diameter	$[m]$
d	Pipe diameter	$[m]$
D_*	Bonneville parameter	$[-]$
D_{50}	Mass median particle diameter: diameter for which 50% is finer	$[m]$
d_H	Hydraulic diameter	$[m]$
E	Erosion flux	$[kg/(m^s \cdot kg)]$
g	Gravitational acceleration	$[m/s^2]$
H	Height of the hopper	$[m]$
h_{bed}	Height of the bed cell	$[m]$
h_{liquid}	Height of the cell above the bed	$[m]$
h_{merged}	Height of the cell after merging	$[m]$
$h_{overflow}$	Height of the water above the overflow	$[m]$
h_{water}	Height of the water above the bed	$[m]$
I	Turbulence intensity	$[-]$
k	Turbulent kinetic energy	$[J/kg]$
L	Length of the hopper	$[m]$
N	Bagnold number	$[-]$
n	Hindered settling exponent	$[-]$
n_0	Porosity	$[m]$
n_k	Hindered settling exponent for fraction k	$[-]$
OV_{cum}	Cumulative overflow losses	$[-]$
OV_{flux}	Overflow flux	$[-]$
P	Production of turbulent kinetic energy	$[J/(kg \cdot s)]$
p	Pressure	$[Pa]$

P_b	Buoyant dissipation of turbulent kinetic energy	$[J/(kg \cdot s)]$
p_{rgh}	Dynamic pressure	$[Pa]$
Q	Flow rate	$[m^3/s]$
q	Flow rate per unit width	$[m^3/(m \cdot s)]$
Q_{in}	Flow rate coming into the hopper	$[m^3/s]$
Q_{out}	Flow rate going out the hopper	$[m^3/s]$
Re	Reynolds number	$[-]$
Re_p	Reynolds particle number	$[-]$
S	Sedimentation flux	$[kg/(m^s \cdot kg)]$
t	Time	$[s]$
U	Depth averaged horizontal velocity	$[m/s]$
u	Horizontal velocity	$[m/s]$
u_*	Shear velocity	$[m/s]$
u_+	Non-dimensional velocity near the wall	$[-]$
v_0	Hopper load parameter	$[m/s]$
v_{sed}	Sedimentation velocity	$[m/s]$
W	Width of the hopper	$[m]$
w	Vertical velocity	$[m/s]$
w_0	Settling velocity single grain	$[m/s]$
w_k	Vertical velocity of fraction k	$[m/s]$
w_s	Hindered settling velocity	$[m/s]$
$w_{0,k}$	Settling velocity single grain of fraction k	$[m/s]$
w_{kr}	Vertical slip velocity of fraction k	$[m/s]$
y_+	Non-dimensional wall distance	$[-]$

1

Introduction

For the Multidisciplinary Project of the master Offshore and Dredging Engineering a literature study is done about the loading of Trailing Suction Hopper Dredgers. The TSHD is a dredging ship that has a full sailing capacity and is used to maintain waterways or reclaim land. From the side of the ship, one or two suction pipes descend to the bottom of the seabed. Due to lower pressure in the pipes, the material at the bed will be sucked inward and discharged in the hopper.
The performance of such a TSHD is described by its production: the amount of sediment loaded in the hopper per unit time. Inherent to the production is the sedimentation in the hopper. The material which does not settle, flows through the overflow. These overflow losses can reach up to 30% of the total volume dredged.
In section 2.1, the flow in the hopper is described. In Paragraph 2.2, a review is given on research about buoyant jets. Research on density current is briefly summarized in Paragraph 2.3. Different relations for settling are given in Paragraph 2.4. In paragraph 2.5, it is explained how to calculate the sedimentation velocity in a hopper. And in Paragraph 2.6, different suspended sediment equations are given.
Several hopper models exist. All these models have their own assumptions and take into account the processes in Figure 2.3 to a greater or lesser extent. In Paragraph 2.7, the different models are discussed.

2

Hopper modelling

2.1. Processes in the hopper

Groot[4] and Van Rhee[10] did laboratory tests with a hopper on model scale. Groot used a hopper of dimensions 3.0 x 0.66 x 0.10 m (L x B x H). During measurements with only water, he measured a logarithmic velocity profile over the height. During measurements with water-sand mixtures, however, there appeared to be a density current at the bottom.

Van Rhee did experiments with a model hopper which had a length of 12 m, a width of 3.08 m and a height of 2.5 m. The maximum overflow level was situated at 2.25 m from the bottom. Just like Groot, a density current was observed at the bottom.

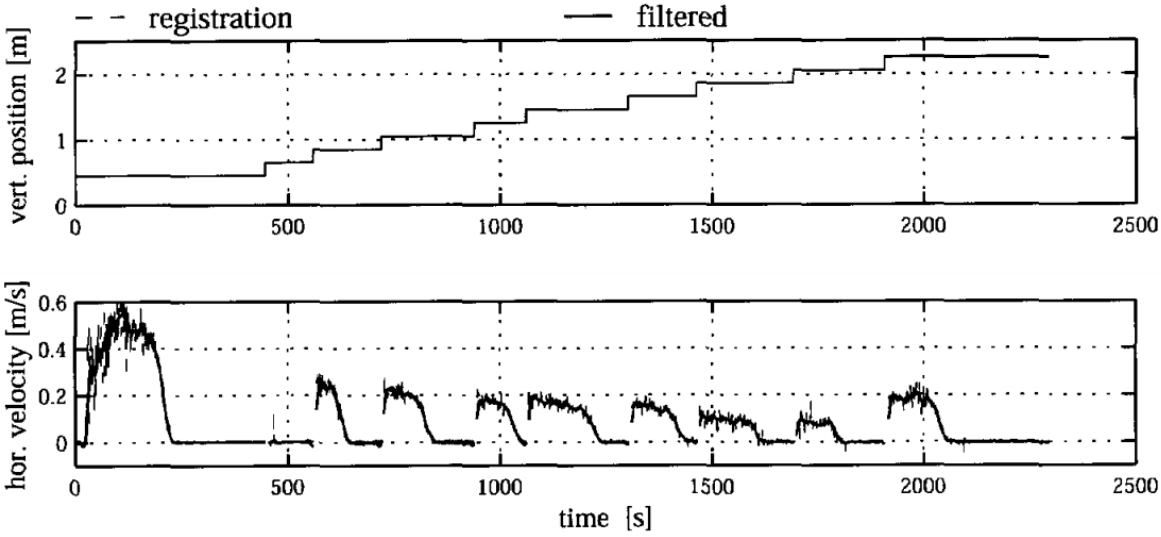

Figure 2.1: Velocity of the density current (Test 8)

The horizontal velocities during Test 8 are shown in Figures 2.1 and 2.2. During the experiment, the EMS was moved over the height. Once the probe was buried, it would be relocated by 20cm in vertical direction.
At the start of the test, the water depth was 1 m and the discharge was about 0.1 m/s. In case of a uniform velocity profile, one could expect a horizontal velocity of $0.1/(1 \cdot 3.08) \approx 0.03 m/s$. Instead, a density current with velocities of up to 0.6 m/s were measured. At the beginning and the end of the loading process, the highest velocities in the density current were measured. This can be seen in

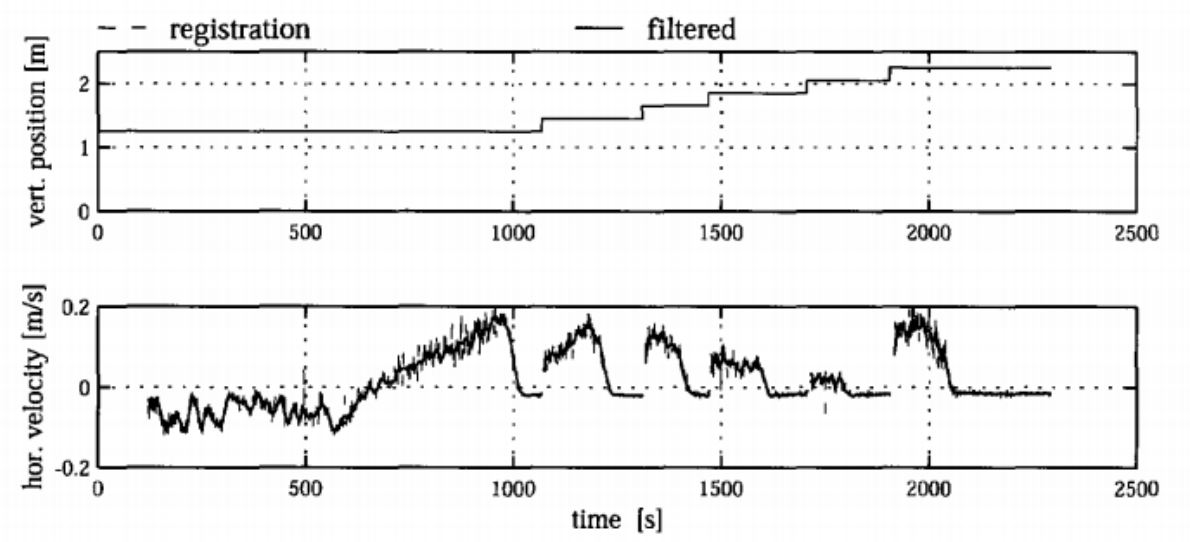

Figure 2.2: Flow field in the hopper (Test 8)

Figure 2.1.

Figure 2.2 is very similar to Figure 2.1, but in Figure 2.2 the instrument was initially located at a larger distance from the bottom(z=1.25 m). A small negative velocity is measured above the density current. This negative velocity is caused by the entrainment of water in the inflowing mixture with a relatively high density.

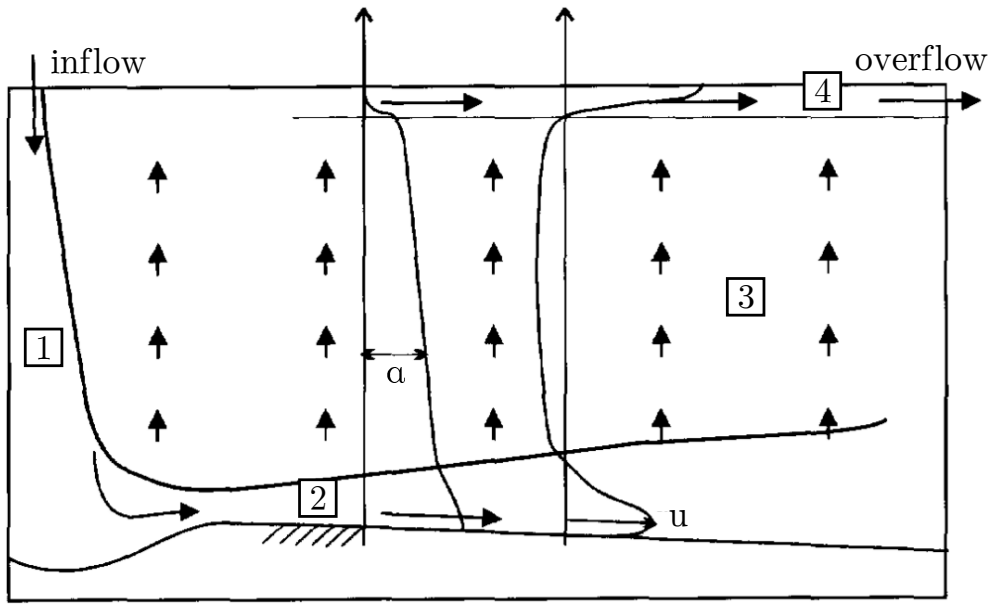

Figure 2.3: Schematic flow field in the hopper with the concentration (α) and horizontal velocity (u) over the height.

Van Rhee gives an overview of the flow in the hopper and the different processes in it (Figure 2.3). In zone 1, a buoyant yet can be found. When the mixture enters the hopper it is denser than its surroundings. The mixture will accelerate towards the bottom. Due to the high velocity and turbulence, an erosion pit is created under the buoyant jet. After leaving the erosion pit, the mixture will flow as a density current over the bottom (zone 2). The interaction between the density current and the bed is important. The bed is rising. The speed with which the bed rises, the sedimentation velocity, depends on the bed shear.

Above the density current (zone 3), the horizontal velocity is in the opposite direction. This is caused by entrainment into the buoyant jet. In vertical direction, the flow is upwards. Depending on the magnitude of this vertical velocity, the particle diameter, the concentration and turbulent diffusion, a particle will move up or down. Zone 4 is a layer of relatively clean water flowing towards the overflow.

In the following sections, a literature study is done about those different processes.

2.2. Buoyant Jets

A buoyant jet is an upward directed jet with lower density than its surroundings. Hence this density difference, an upward buoyant force is exerted on the jetted fluid. The situation in the hopper is the same but upside down.
In literature, distinction is made between circular and planar jets. It can be assumed that the jet in the hopper is planar.

Rodi[15] gives a good relation for planar buoyant jets mainly based on the experiments of Kotsovinos[17]. Kotsovinos did experiments on planar jets with an inlet of 20x130mm. This is considerably smaller than the planar jet in the hopper. This could cause inaccuracy.
Yannopoulos[16] has derived a relation based on the experiments of Ramaprian & Chandrasekhara[18]. The inlet of the experimental setup of Ramaprian & Chandrasekhara was 5x250mm. This is again smaller than the situation in the hopper.
Yannopoulos distinguishes two regimes: the jet regime and the plume regime. The jet regime is close to the inlet where the flow is still accelerating or decelerating. Further away from the inlet, the buoyancy force becomes equal to the friction force. The velocity then becomes constant. This is the plume regime. In his simulations, Van Rhee observed that the velocity at the bottom of the jet is independent of the inlet velocity (for constant discharge). This means that the plume regime is reached at the bottom of the hopper. The relations of Yannopoulos are more convenient than the relations of Rodi, since also the concentrations can be calculated with Yannopoulos. In the plume regime the velocity can be calculated as follows:

$$\frac{w_c}{w_0} = A_p F_0^{-\frac{2}{3}} \tag{2.1}$$

w_c is the centre line velocity and w_0 the inlet velocity. F_0 is the Froude number:

$$F_0 = \frac{w_0}{\sqrt{9.81 d \frac{\rho_0 - \rho_a}{\rho_a}}} \tag{2.2}$$

In which ρ_0 is the density at the inlet and ρ_a the density of the surroundings. d is the width of the inlet.

$$A_p = \left(\frac{2Y}{\sqrt{\pi}} \frac{\sqrt{K_c}}{\lambda_M \lambda_B} \right)^{\frac{1}{3}} K_w^{-\frac{1}{2}} \tag{2.3}$$

Also the centre line concentration can be calculated:

$$\frac{\alpha_c}{\alpha_0} = B_p F_0^{\frac{2}{3}} \frac{z}{d} \tag{2.4}$$

$$B_p = \left(\frac{\lambda_M}{\lambda_B^2} \frac{Y^2 \sqrt{2}}{\pi K_c^2} \right)^{\frac{1}{3}} \tag{2.5}$$

In the hopper, the jet is influenced by the wall. Unfortunately, no thorough research has been done on buoyant wall jets. By assuming that the wall acts as a symmetry plane with no friction, the equations above can still be used.

Table 2.1: Input parameters for Equations 2.3 and 2.5

λ_M	1.1
λ_B	1.18
λ	1.21
K_w	0.132
K_c	0.160
Y	1.01

2.3. Density Currents

An important research on density currents is the research of Parker[19]. By using the so called top-hat assumption, Parker derived balances for the mass, momentum and concentration:

$$\frac{\delta h}{\delta t} + \frac{\delta U h}{\delta x} = w_e \tag{2.6}$$

$$\frac{\delta C h}{\delta t} + \frac{\delta U C h}{\delta x} = -v_{sed}(1 - n_0 - \alpha_b) + w_e \alpha_a \tag{2.7}$$

$$\frac{\delta U h}{\delta t} + \frac{\delta U^2 h}{\delta x} = -1/2 \Delta g \frac{\delta C h^2}{\delta x} + \Delta g C h \tan(\beta) - u_*^2 \tag{2.8}$$

u_* is the shear velocity.
w_e is the entrainment velocity and can be calculated with: $w_e = e_w * U$.
α_b is the near bed concentration and can be calculated with: $\alpha_b = r_0 * C$.
α_a is the concentration above the density current.
β is the slope.
Δ is the submerged specific gravity: $\frac{\rho_s - \rho_w}{\rho_w}$.
For the calculation of r_0 and e_w, the reader is directed to the article of Parker[19].

The top-hat assumption means that the velocity and concentration are constant over the height of the density current. Therefore U and C are the mean values. In reality, the velocity and concentration vary over the height of the density current. Recently, a lot of research has been done to shape factors. For example, Sequeiros[20] measured the shape factors for different flow regimes. Equations 2.6, 2.7 and 2.8 then have to be adjusted slightly to add the shape factors.

2.4. Settling

The settling velocity is an important parameter for hopper flow. However, finding a good formulation of the settling velocity is difficult. The settling velocity of a single grain in a quiescent surrounding fluid, the terminal settling velocity, can be derived by using the balance of gravity and drag. The following formula can be obtained:

$$w_0 = -\sqrt{\frac{4 g \Delta D \Psi}{3 C_D}} \tag{2.9}$$

Δ is the specific density and is defined as $(\rho_s - \rho_w)/\rho_w$. Ψ is the shape factor and is a correction for the difference of nominal and sieve diameter. The drag depends on the frontal surface which can be calculated with the sieve diameter. The gravity force is calculated with the nominal diameter. Therefore, Ψ is defined as:

$$\Psi = \frac{M_{grain}}{\rho_s \frac{\pi}{6} D_{sieve}^3} \tag{2.10}$$

For perfect spheres the shape factor is exactly 1. For sand grains it is around 0.7.

The C_D in Equation 2.11 depends on the Reynolds Particle Number:

$$Re_p = \frac{w_0 D}{\nu} \tag{2.11}$$

For perfect spheres the following empirical relations for C_D are found:

$$\begin{aligned} Re_p \leq 1 \quad &\rightarrow \quad C_D = \tfrac{24}{Re_p} \\ 1 < Re_p < 2000 \quad &\rightarrow \quad C_D = \tfrac{24}{Re_p} + \tfrac{3}{\sqrt{Re_p}} + 0.34 \\ Re_p \geq 2000 \quad &\rightarrow \quad C_D = 0.4 \end{aligned} \tag{2.12}$$

The formula of C_D for the laminar region and the turbulent region can be substituted into Equation 2.11. This gives for the laminar region:

$$w_0 = -\frac{\Psi \Delta g D^2}{18\nu} \tag{2.13}$$

And for the turbulent region this gives:

$$w_0 = -1.8\sqrt{\Psi \Delta g D} \tag{2.14}$$

The transition regime has to be solved iteratively.

It can be questioned if solving the settling velocity iteratively with Equations 2.11 and 2.12 gives a correct outcome for natural grains since Equation 2.12 is the drag coefficient for perfect spheres. Numerous experiments have been done to arrive at similar formulations for natural grains. For example Cheng[36] compared different researches. The papers he compared mainly arrived at drag coefficients of approximately $32/Re_p$ and 1.1 for the Stokes and turbulent regime, respectively . Cheng didn't use the form factor in Equation 2.11. This then gives:

$$w_0 = -\frac{\Delta g D^2}{24\nu} \qquad \text{and} \qquad w_0 = -1.1\sqrt{\Delta g D} \tag{2.15}$$

For the laminar region, Cheng and the iterative method with $\Psi = 0.7$ correspond very well. For the turbulent regime they differ. Cheng also made a fit which can be used explicitly over the whole range of diameters:

$$\frac{w_0 d D}{\nu} = -\left(\sqrt{25 + 1.2 D_*^2} - 5\right)^{1.5} \tag{2.16}$$

Ferguson and Church[37] also compared different researches and added some experiments of their own. After fitting the data, they arrived at the following empirical formula:

$$w_0 = -\frac{\Delta g D^2}{C_1 \nu + (0.75 C_2 \Delta g D^3)^{0.5}} \tag{2.17}$$

This formula is valid for all regimes. For perfectly round particles the $C_1 = 18$ and $C_2 = 0.4$. For natural grains, Ferguson and Church advise $C_1 = 18$ and $C_2 = 1.0$ when the sieve diameter is used and $C_1 = 20$ and $C_2 = 1.1$ when the nominal diameter is used.

Another emperical relation is the relation of Ruby and Zanke:

$$w_0 = -\frac{10\nu}{D}\left(\sqrt{1 + \frac{\Delta g D^3}{100\nu^2}} - 1\right) \tag{2.18}$$

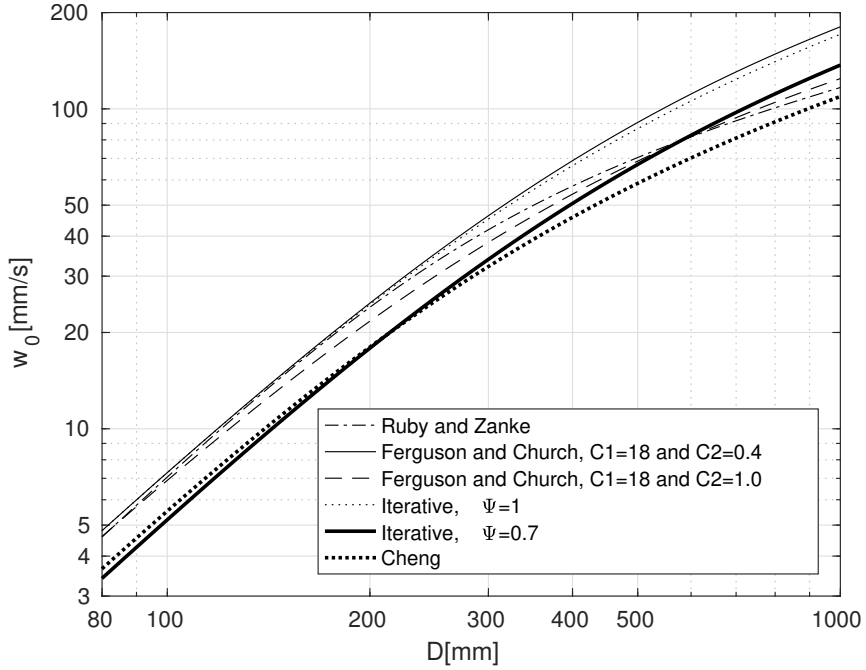

Figure 2.4: Grain diameter versus terminal settling velocity with $\nu = 1.11 \cdot 10^{-6}$ m^2/s

The equations described above are plotted in Figure 2.4. The first thing which can be seen is that the settling velocities for perfect spheres calculated with Ferguson and Church and with the iterative method ($\Psi = 1$) are very similar. Secondly, it can be observed that both empirical relations for natural grains, Ferguson & Church and Ruby & Zanke, are also similar. However, they differ with the findings of Cheng.
All in all, it can be concluded that it is hard to estimate the settling velocity. Each excavation site has its own type of sand with its own shape. This gives large variation is settling velocities. The estimation of the settling velocity will probably be the highest contribution to inaccuracy of the model. As can be seen in Figure 2.4, particles with the same diameter but different grain shapes can easily differ 20% in settling velocity.

textbfHindered Settling
For an increased volume concentration, the settling velocity decreases due to an increasing drag caused by water flowing upwards. This is called hindered settling and can be described by the relation of Richardson and Zaki[38]:

$$w_s = w_0(1-\alpha)^n \tag{2.19}$$

Based on experiments Richardson and Zaki found values for n:

$$\begin{aligned} Re_p \leq 0.2 \quad &\rightarrow \quad n = 4.65 \\ 0.2 < Re_p < 1 \quad &\rightarrow \quad n = 4.35 Re_p^{-0.03} \\ 1 < Re_p < 200 \quad &\rightarrow \quad n = 4.45 Re_p^{-0.1} \\ Re_p \geq 200 \quad &\rightarrow \quad n = 2.39 \end{aligned} \tag{2.20}$$

Two more convenient relations are the relations of Rowe and Garside & Al-Dibouni:

$$n = \frac{a + bRe_p^{\alpha}}{1 + cRe_p^{\alpha}} \tag{2.21}$$

Table 2.2: Constants hindered settling

Author	Re_p	Concentration	a	b	c	α
Richardson & Zaki	$0.000185 < Re_p < 7150$	$0.05 < \alpha < 0.65$	-	-	-	-
Garside & Al-Dib.	$0.001 < Re_p < 3 \cdot 10^4$	$0.04 < \alpha < 0.55$	5.1	0.27	0.1	0.9
Rowe	$0.2 < Re_p < 1 \cdot 10^3$	$0.04 < \alpha < 0.55$	4.7	0.41	0.175	0.75

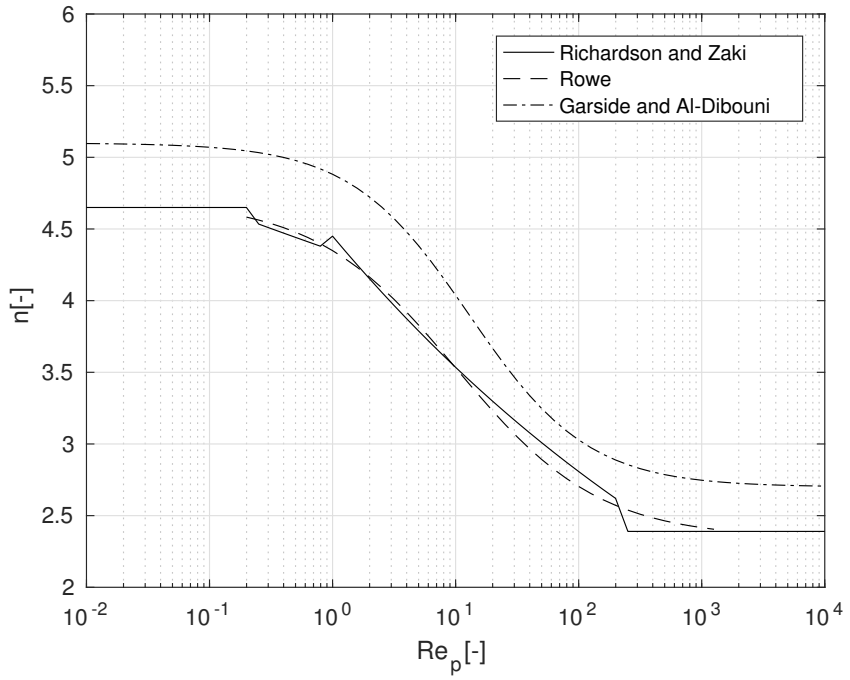

Figure 2.5: Reynolds Particle Number versus the exponent for hindered settling

The relation of Rowe has a smaller range for Re_p than Garside & Al-Dibouni and Richardson & Zaki, but for this thesis that is not a problem. For particles of D=60μm the Re_p is approximately 0.2 and for D=1000μm the Re_p is approximately 100.

Both Richardson & Zaki and Garside & Al-Dibouni developed their equations by doing experiments with monodisperse perfect spheres. It appears that the shape of the particles has influence on the hindered settling effect. Generally, it is found that for natural sand the exponent is slightly higher than Richardson & Zaki[40][41]. Just like with the settling velocity, with the determination of the hindered settling is causing a lot of inaccuracy.

2.5. Sedimentation and Erosion

The sedimentation in a hopper occurs under high concentration. Van Rhee[10] executed closed flume experiments to determine the effect of the bed shear on the sedimentation velocity for high near bed concentrations.

Every experiment started by pumping a concentrated mixture at a higher velocity than the deposition velocity through the circuit. The deposition velocity is the velocity at which a stationary bed is formed in a pipe, so at the beginning of every experiment no stationary bed was present in the circuit. Parallel to the section in Figure 2.6, a bypass was installed. By partly closing the butterfly valve, the velocity in the measurement section decreased and the flow rate in the bypass increased. Hence this suddenly decreased velocity, sedimentation started to occur. By measuring the conductivity it could be measured

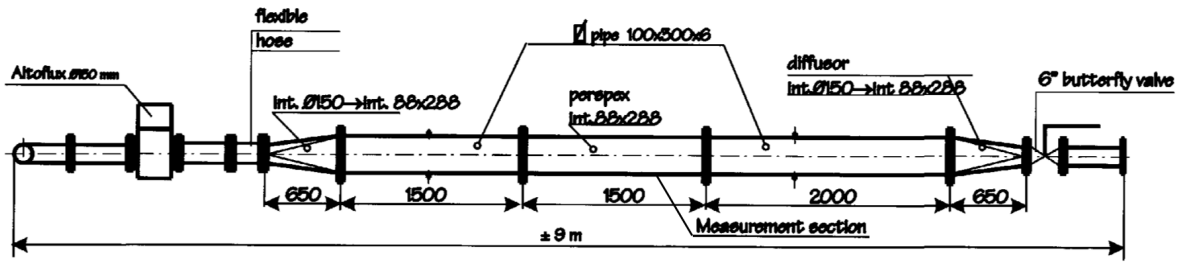

Figure 2.6: Side view of the test arrangement (mixture flows from right to left)

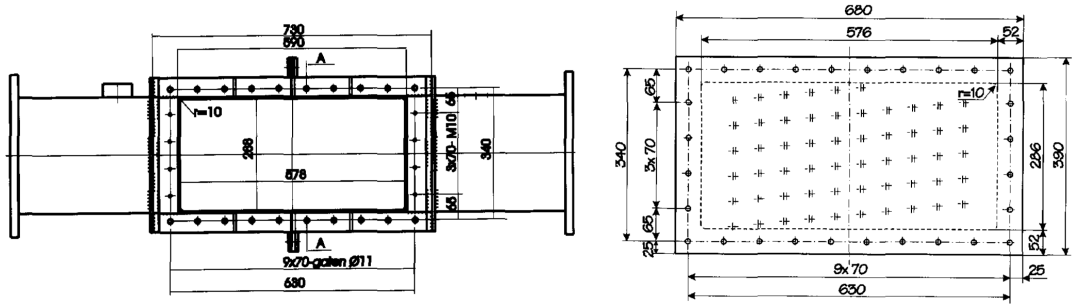

Figure 2.7: Measurement section (left) and a close-up of the arrangement of the conductivity probes (right)

when the bed-surface passed a probe. All probes were placed at different vertical position from the bottom. By measuring the time difference of the passing of the bed between probes, the sedimentation velocity was calculated. The time difference for both probes 1 and 3 and probes 2 and 4 was measured.

Table 2.3: Height of the probes above the bottom

probe	z[mm]
1	5
2	10
3	15
4	20

Van Rhee noted that the sedimentation velocities between probes 1 and 3 were a bit lower than the sedimentation velocity between probes 2 and 4, since the measurements with probes 1 and 3 were still influenced by the decreasing flow velocity. Therefore, Van Rhee only used probes 2 and 4.

To test the influence of the initial velocity, experiments were done for both low and high initial velocities. The low and high velocities before partly closing the valve were respectively 2.7 and 3.7 m/s. In Figure 2.8 the PSDs of the different sands are shown.

An important parameter for the sedimentation velocity is the bed porosity. It appeared that the packing of the grains depends on the flow velocity at which sedimentation occurs. For the sand with $D_{50} = 125\mu m$, the following fit could be made:

$$\alpha_{max} = 0.495 + 0.085U \tag{2.22}$$

Figure 2.10 shows the measured sedimentation velocity versus the Shields parameter. v_{sed0} is the sedimentation velocity without bed shear. The Shields parameter is a measure for the shear stress

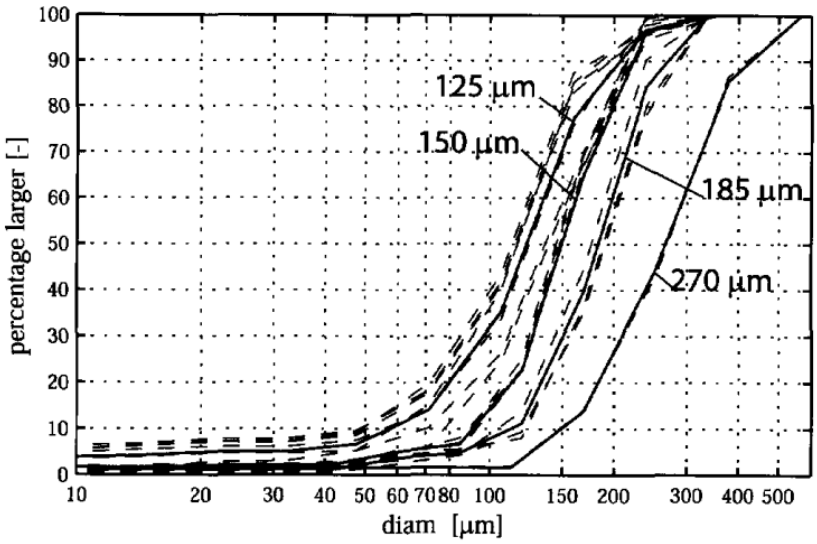

Figure 2.8: Particle Size Distributions of the sand used in the experiments

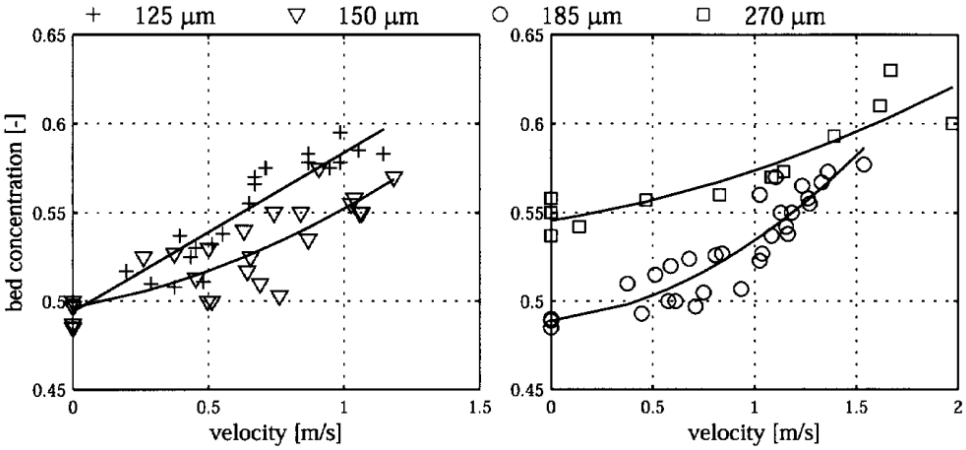

Figure 2.9: Bed concentration versus velocity

versus gravity force and is defined by:

$$\theta = \frac{\tau}{(\rho_s - \rho_w)gD} = \frac{u_*^2}{g\Delta D} \tag{2.23}$$

For D the D_{50} is used, $\Delta = (\rho_s - \rho_w)/\rho_w$. It can be seen that the sedimentation velocity decreases for higher Shields parameters:

$$R(\theta, c_b) = \frac{v_{sed}}{v_{sed,0}} = \begin{cases} 1 - \frac{\theta}{\theta_0} & \text{for } \theta \leq \theta_0 \\ 0 & \text{for } \theta > \theta_0 \end{cases} \tag{2.24}$$

In which θ_0 is approximately 4.5. The sedimentation velocity can then be calculated with:

$$v_{sed} = R(\theta, \alpha_b) v_{sed,0} = R(\theta, \alpha_b) \frac{-\alpha_b w_s}{1 - n_0 - \alpha_b} \tag{2.25}$$

Equation 2.24 is, however, a very rough fit of Figure 2.10. Some measurements are far removed from this fit.

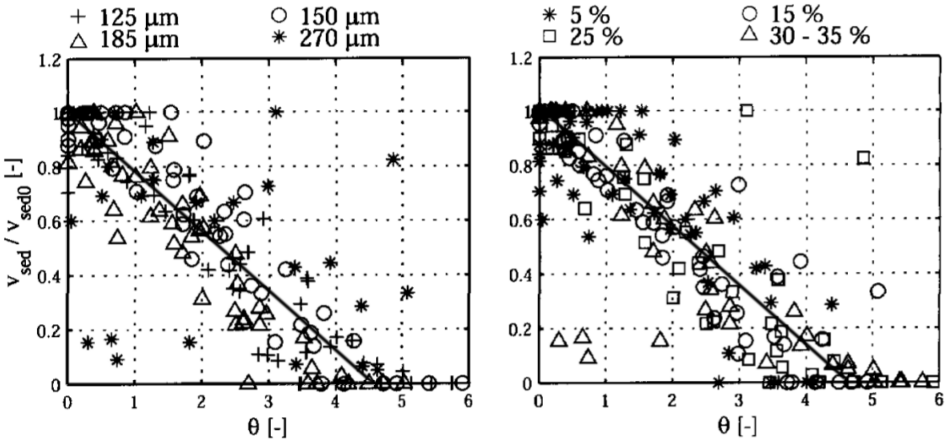

Figure 2.10: Relative sedimentation velocity versus Shields parameter

An frequently used expression for the sedimentation velocity is:

$$v_{sed} = \frac{S - E}{\rho_s(1 - n_0 - \alpha_b)} \tag{2.26}$$

In which S is the sedimentation flux[$kgm^{-2}s^{-1}$], E is the erosion flux[$kgm^{-2}s^{-1}$], ρ_s is the density of the particles[kgm^{-3}], n_0 is the porosity[-] and α_b is the near bed concentration[-]. The settling flux is determined by:

$$S = -\rho_s \alpha_b w_s \tag{2.27}$$

Where w_s is the hindered settling velocity[m/s]. The erosion flux can be calculated with the empirical pick-up function of Van Rijn[30]:

$$\Phi_p = \frac{E}{\rho_s\sqrt{g\Delta D}} = 0.00033 D_*^{0.3}\left(\frac{\theta - \theta_{cr}}{\theta_{cr}}\right) \tag{2.28}$$

In which Φ_p is the pickup flux[-] and D_* is the Bonneville parameter:

$$D_* = D\sqrt[3]{\frac{\Delta g}{\nu^2}} \tag{2.29}$$

ν is the kinematic viscosity of the ambient fluid[m^2/s]. The critical Shields parameter θ_{cr} can be read out of the Shields curve or calculated by one of the several fits. For example Brownlie[31]:

$$\theta_{cr} = 0.2 Re_p^{-0.6} + 0.06 e^{-17.77 Re_p^{-0.6}} \tag{2.30}$$

The Particle Reynolds number, Re_p, is a measure of the particle inertia forces versus viscous forces:

$$Re_p = \frac{D\sqrt{\Delta g D}}{\mu} \tag{2.31}$$

By estimating the settling flux (2.27), the pickup flux was obtained (Figure 2.11). A large difference between the pick function of Van Rijn and the measurements can be seen. In the experiments of Van Rijn, the maximum concentration was nearly zero. Figure 2.11 clearly shows the influence of the near bed concentration.

In a recent article about breaching, Van Rhee[33] gives a pickup function which depends on the near bed concentration:

$$\Phi_p = A\frac{1 - n_0 - \alpha_b}{1 - n_0}\frac{\theta}{\theta'_{cr}} \tag{2.32}$$

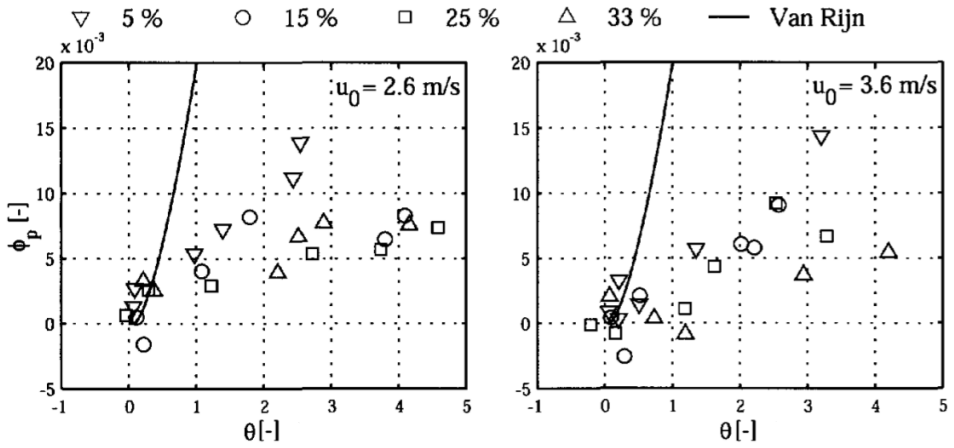

Figure 2.11: Measurements of Van Rhee under high concentration ($125\mu m$) and the pickup function of Van Rijn (2.28)

In which A is 0.000616 and θ'_{cr} can be caculated with:

$$\theta'_{cr} = \theta_{cr}\left(\frac{\sin(\phi-\beta)}{\sin(\phi)} + \frac{v_e}{k_l}\frac{n_l - n_0}{1-n_l}\frac{1}{\Delta(1-n_0)}\right) \tag{2.33}$$

θ_{cr} is the critical Shields value calculated with Equation 2.31. The first term between the brackets is the influence of the slope on the critical Shields value. β is the slope angle and ϕ is the angle of internal friction. The slope angle is positive when the mixture is running down the slope (Figure 2.12).
The second term in Equation 2.33 is the effect of dilatancy, which is important for $v_e >> k_l$, i.e. high speed erosion. v_e and k_l are the erosion speed and permeability, respectively. Since in a hopper $\frac{v_e}{k_l}$ is smaller than 3, the second term can be assumed to be zero.

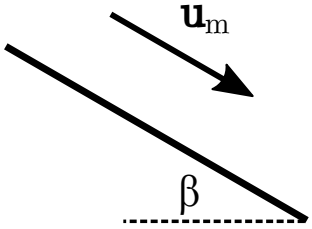

Figure 2.12: Positive slope angle.

2.6. Suspended sedimentation transport

Multi-phase flow can be found everywhere in nature and engineering. Different two-phase flows which can be found are solid-liquid, solid-gas, liquid-gas or two immiscible fluids. This thesis is about the multi-phase flow which falls into the category of solid-liquid flow, also called suspended sedimentation transport. Suspended sedimentation transport can be divided in two types of modelling: Lagrangian and Eulerian.

Lagrangian
The difference between these two types of modelling lies in the choice of reference frame. With Lagrangian modelling the reference frame is following the individual particles. The trajectory of every particle is described by Newton's second law. This means the trajectory of every particle can be determined. The advantage of this approach is it's accuracy. The influence of the particle on the surrounding liquid can accurately be calculated, but also the particle-particle interactions can be calculated precisely. A disadvantage is the calculation effort needed when the amount of particles is big. Therefore this approach is mainly used when particles are relatively big compared to the fluid domain.

Eulerian
In the Eulerian approach the reference frame is chosen to be fixed. To calculate the velocity of every phase, the continuity and momentum equation is solved for each phase. This can only be done if the characteristics of the particles can be described as a continuum. This is only possible for small particles. It can be questioned if continuum holds for coarse sand or gravel. To simulate gravel the

Lagrangian method could be needed. Luckily, we know that coarse sand or gravel directly settles on the bed. To calculate the overflow losses, particle diameters from approximately 70 to 400 μm are of interest. Particles of this size are small enough to simulate with an Eulerian approach.

Also the Eulerian approach can be subdivided into different types: Euler-Euler and Drift Flux.

2.6.1. Euler Euler

Every fraction is denoted by its value of k. Then it follows:

$$\alpha_k = \frac{V_k}{V_0} \tag{2.34}$$

Here α_k is the concentration of fraction k. V_k is the volume of fraction k and V_0 is the total volume. If the concentrations of the different fractions are summed we get:

$$\sum_{k=1}^{N} \alpha_k = 1 \tag{2.35}$$

In the Euler Euler approach, every fraction has its own continuity and momentum equation:

$$\frac{\partial \alpha_k \rho_k}{\partial t} + \nabla \cdot \alpha_k \rho_k \mathbf{u}_k = 0 \tag{2.36}$$

$$\frac{\partial \alpha_k \rho_k \mathbf{u}_k}{\partial t} + \nabla \cdot (\alpha_k \rho_k \mathbf{u}_k \mathbf{u}_k) = -\nabla \alpha_k p_k + \nabla \cdot \left(\alpha_k \mathbf{T}_k + \alpha_k \mathbf{T}_k^t \right) + \alpha_k \rho_k \mathbf{g} + \alpha_k \mathbf{m}_k \tag{2.37}$$

$\mathbf{T}_k$ and $\mathbf{T}_k^t$ are the contributions of the viscous and turbulent stresses, respectively. $\mathbf{T}_k$ is expressed as follows:

$$\mathbf{T}_k = \mu_m \left(\nabla \mathbf{u}_k + \nabla \mathbf{u}_k^T - \frac{2}{3} \nabla \cdot \mathbf{u}_k \mathbf{I} \right) \tag{2.38}$$

Normally for incompressible flow, the third term is omitted, but since $\nabla \cdot \mathbf{u}_k \neq 0$ this is not possible for suspended sediment transport. The calculation of $\mathbf{T}_k^t$ depends on the turbulence modelling.

$\mathbf{m}_k$ represents the momentum transfer between the phases. The challenge with Euler Euler is the determination of this momentum transfer. Incorrect calculation of the momentum transfer easily leads to numerical instabilities and inaccuracy. When correctly used, an Euler-Euler approach is more accurate than the Drift Flux.

2.6.2. Drift Flux

With a Drift Flux model, the mixture is considered as a whole instead of several separate phases. The continuity equation is obtained, by adding the the continuity equations of the different phases.

$$\frac{\partial \rho_m}{\partial t} + \nabla \cdot \rho_m \mathbf{u}_m = 0 \tag{2.39}$$

The mixture density can be calculated with:

$$\rho_m = \sum_{k=1}^{N} \alpha_k \rho_k \tag{2.40}$$

Also the mixture momentum equation is obtained by adding the the momentum equations of the different phases:

$$\frac{\partial \rho_m \mathbf{u}_m}{\partial t} + \nabla \cdot (\rho_m \mathbf{u}_m \mathbf{u}_m) = -\nabla p_m + \nabla \cdot \left(\mathbf{T}_m + \mathbf{T}_m^t - \sum_{k=1}^{N} \alpha_k \rho_k \mathbf{u}_{km} \mathbf{u}_{km} \right) + \rho_m \mathbf{g} \tag{2.41}$$

For the derivation of Equations 2.49 and 2.41, the reader is directed to Appendix A of Brennan[21]. From adding the momentum equations of the different fractions, it also follows that:

$$\mathbf{u}_m = \frac{\sum_{k=1}^{N} \alpha_k \rho_k \mathbf{u}_k}{\rho_m} \tag{2.42}$$

This is called the *mixture centre of mass velocity*.

When the different momentum equation are added the term $\alpha_k \mathbf{m}_k$ cancels out. Every force of each phase exerts an opposite force to another phase, so $\sum_{k=1}^{N} \alpha_k \mathbf{m}_k = 0$. This is very convenient and makes Drift Flux easier to apply than Euler Euler.

$\mathbf{T}_m$ and $\mathbf{T}_m^t$, again, are the contribution of the viscous and turbulent stresses respectively. $\mathbf{T}_m$ is calculated as follows:

$$\mathbf{T}_m = \mu_m \left(\nabla \mathbf{u}_m + \nabla \mathbf{u}_m^T - \frac{2}{3} \nabla \cdot \mathbf{u}_m \mathbf{I} \right) \tag{2.43}$$

The concentration of the different fraction are determined with the advection-diffusion equation:

$$\frac{\partial \alpha_k}{\partial t} + \nabla \cdot (\alpha_k \mathbf{u}_k) = \nabla \cdot (\Gamma_t \nabla \alpha_k) \tag{2.44}$$

In which Γ_t is the turbulent diffusion coefficient and $\mathbf{u}_k$ the fraction velocity. Goeree[23] derived a formula for the fraction velocity:

$$\mathbf{u}_k = \mathbf{u}_m + \mathbf{u}_{km} = \mathbf{u}_m + \mathbf{u}_{kr} - \sum_{k=1}^{N} c_k \mathbf{u}_{kr} \tag{2.45}$$

The mass fraction, c_k can be calculated with:

$$c_k = \frac{\rho_k \alpha_k}{\rho_m} \tag{2.46}$$

The slip velocity $\mathbf{u}_{kr}$ is the velocity of a fraction compared to the fluid phase:

$$\mathbf{u}_{kr} = \mathbf{u}_k - \mathbf{u}_f \tag{2.47}$$

In horizontal direction this is assumed to be zero. In vertical direction it is:

$$w_{kr} = w_{0,k} \left(1 - \alpha_t\right)^{n_k - 1} \tag{2.48}$$

Note that $w_{0,k}$ is negative.

2.6.3. *Mixture centre of mass velocity* and *mixture flux velocity*

For the derivation of the pressure equation, the continuity equation is needed. As explained earlier, the correct continuity equation for the *mixture centre of mass velocity*, $\mathbf{u}_m$, is:

$$\frac{\partial \rho_m}{\partial t} + \nabla \cdot \rho_m \mathbf{u}_m = 0 \tag{2.49}$$

This means:

$$\nabla \cdot \mathbf{u}_m \neq 0 \tag{2.50}$$

However, very often, still $\nabla \cdot \mathbf{u} = 0$ is assumed. When $\nabla \cdot \mathbf{u} = 0$ is assumed not the *mixture centre of mass velocity*, but the *mixture flux velocity* is calculated:

$$\mathbf{j}_m = \sum_{k=1}^{N} \alpha_k \mathbf{u}_k \tag{2.51}$$

For $\mathbf{j}_m$ indeed the following continuity equation is valid:

$$\nabla \cdot \mathbf{j}_m = 0 \tag{2.52}$$

Although, the results between usage of $\mathbf{j}_m$ and $\mathbf{u}_m$ do not differ that much, it is incorrect to use $\mathbf{j}_m$. Furthermore with $\mathbf{j}_m$, Equation 2.45 cannot be used, since $\mathbf{u}_m$ is unknown. Instead, the following equation for the fraction velocity needs to be used:

$$\mathbf{u}_k = \mathbf{j}_m + \mathbf{u}_{kj} = \mathbf{j}_m + \mathbf{u}_{kr} - \sum_{k=1}^{N} \alpha_k \mathbf{u}_{kr} \tag{2.53}$$

The slip velocity, $\mathbf{u}_{kr}$, can still be calculated with Equation 2.48.

2.6.4. Turbulence modelling

The starting point for turbulence modelling is separating the velocity into a main velocity and velocity fluctuation:

$$\mathbf{u} = \overline{\mathbf{u}} + \mathbf{u}' \tag{2.54}$$

By substituting this into the Navier-Stokes equation(Equations 2.41 and 2.37) and doing some derivations, it can be found that:

$$\mathbf{T}^t = -\rho \overline{\mathbf{u}'\mathbf{u}'} \tag{2.55}$$

Since its effect on the mean flow is like that of a stress term, this term is known as the Reynolds stress. The vertices transport momentum across the fluid. When a velocity gradient is present in the mean flow, faster moving layers will be decelerated and slower layers will be accelerated due to this transport of momentum.

To obtain equations containing only the mean velocity and pressure, we need to close the momentum equations by modelling the Reynolds stress term. This is called the closure problem. Boussinesq was the first to attack the closure problem, by introducing the concept of eddy viscosity. The relation he proposed is called the Boussinesq hypothesis:

$$-\rho \overline{\mathbf{u}'\mathbf{u}'} = \mu_t \left(\nabla \mathbf{u} + \nabla \mathbf{u}^T \right) - \frac{2}{3} \left(\mu_t \nabla \cdot \mathbf{u} + \rho k \right) \mathbf{I} \tag{2.56}$$

In which k is the turbulent kinetic energy and is defined by $k = \frac{1}{2}(\overline{u'^2} + \overline{v'^2} + \overline{w'^2})$. The calculation of this eddy viscosity μ_t depends on the type of turbulence modelling. The various types of turbulence modelling can be divided into three main groups:

Direct Numerical Simulation (DNS)
With DNS, actually, no turbulence is modelled, so $\mathbf{T}^t$ and μ_t are zero. This means all turbulent scales must be resolved down to the Kolmogorov scale. At the Kolmogorov scale, viscosity dominates and the turbulent kinetic energy is dissipated into heat. A very fine mesh is needed to simulate these small scales. For this reason, DNS is only used for the purpose of research.

Large Eddy Simulation (LES)
With LES, only the large eddies are resolved. The smaller scales need to be modelled and are represented by an additional stress, which is called the Sub-Grid-Scale (SGS) stress. To calculate this SGS stress a turbulence model is required. A model which is frequently used nowadays is the Wall Adapting Local Eddy (WALE) viscosity model. The eddy viscosity, obtained with the SGS model, can be substituted in Equation 2.56.

Reynolds Averaged Navier-Stokes (RANS)
In RANS all turbulent scales, large and small, are modelled. Again, a turbulence model is needed to model those turbulent scales. Contrary to DNS and LES, where simulation need to be done in 3D, simulating in 2D is also possible with RANS. The most basic turbulence model is Prandtl's mixing length model. In the Prandtl's mixing length model, the spatial variation of the eddy viscosity is assumed to be known on forehand.
If the spatial variation of the eddy viscosity is unknown, a more advanced method is required. The two-equation turbulence models are frequently used. These models consist of two additional transport equations. The first equation is for the turbulent kinetic energy k. The second equation is for the dissipation rate ϵ or the specific dissipation rate ω. The dissipation rate ϵ is the rate at which the turbulent kinetic energy dissipates into heat. The specific dissipation rate ω is defined as ϵ/k. An overview of the different two-equation models can be seen in appendix A.

2.6.5. Turbulent boundary layers

A lot of research has been done about the flow close to the wall e.g., Chieng & Launder[24], Patel, Rodi & Scheuerer[25], Cebeci & Smith[26]. To describe the flow near the wall, a certain division in regions is used:

- Inner layer:
  - Viscous region
  - Buffer region
  - Log-law or inertial region
- Defect layer

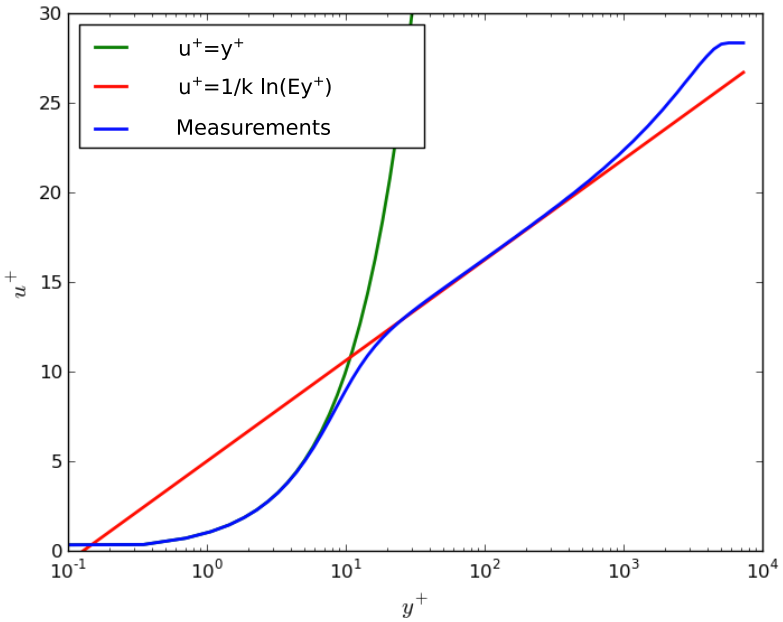

Figure 2.13: Velocities near the wall

RANS-models are not able to simulate the flow in the inner layer. Boundary conditions for k, ϵ, ω and μ_t need to be applied to model the flow in the inner layer.
The viscous region is the area with an $y+$ smaller than 5. In the viscous region the following relation can be found:

$$u_+ = y_+ \tag{2.57}$$

In which u_+ and y_+ are the non-dimensional velocity and distance:

$$u_+ = \frac{u}{u_*} \tag{2.58}$$

$$y_+ = \frac{u_* y}{\nu} \tag{2.59}$$

$$u_* = \sqrt{\frac{\tau}{\rho}} \tag{2.60}$$

The log-law region is the region with approximately $30 < y_+ < 100$. The upper limit depends on the Reynolds number, but an y_+ of 100 is often chosen as the upper limit. For the log-law region another relation is valid:

$$u_+ = \frac{1}{\kappa} \ln (y_+) + B \tag{2.61}$$

κ is 0.40 and B is experimentally found to be between 4.9 and 5.7 for smooth walls. This formula is often written in the following form:

$$u_+ = \frac{1}{\kappa} \ln (E y_+) \tag{2.62}$$

E is then between 7.0 and 9.8. A lot of a CFD-packages use a value of 9.8.

For walls with a dimensionless roughness, k_s^+, above 90 a value of ΔB has to be subtracted:

$$\Delta B = \frac{1}{\kappa} \ln \frac{k_s u_*}{\nu} - 3.3 = \frac{1}{\kappa} \ln k_s^+ - 3.3 \tag{2.63}$$

This can be subtracted from 2.62:

$$u_+ = \frac{1}{\kappa} \ln (E y_+) - \frac{1}{\kappa} \ln (k_s^+) + 3.3 \tag{2.64}$$

$$u_+ = \frac{1}{\kappa} \ln \frac{E y_+}{k_s^+} - \frac{1}{\kappa} \ln e^{-3.3\kappa} \tag{2.65}$$

$$u_+ = \frac{1}{\kappa} \ln \frac{E y_+}{e^{-3.3\kappa} k_s^+} \tag{2.66}$$

$$u_+ = \frac{1}{\kappa} \ln \frac{E y_+}{0.27 k_s^+} \tag{2.67}$$

Most CFD-packages use a formula which looks like:

$$u_+ = \frac{1}{\kappa} \ln \frac{E y_+}{1 + C k_s^+} \tag{2.68}$$

This is a very convenient formulation. For rough walls ($k_s^+ > 90$) $C k_s^+$ is a lot bigger than one. Equation 2.68 then gives the same outcome as Equation 2.67. And for smooth walls (k_s^+=0) Equation 2.68 gives

the same outcome as Equation 2.62. Ansys uses a value of C=0.3[34]. With this value of 0.3, one will attain the exact same formula as Van Rhee[10]uses for rough walls:

$$u_+ = \frac{1}{\kappa} \ln \frac{9.8 y_+}{0.3 k_s^+} = \frac{1}{\kappa} \ln \frac{32 y}{k_s} \tag{2.69}$$

Simulations which make use of Equation 2.57 are called low-Reynolds simulations. To get an y_+ smaller than 5, the distance between the cell centre of the first cell and the wall needs to be very small. Therefore, in low-Reynolds simulations a grading of the cell size near the wall is used. This causes the calculation time of low-Reynolds to be relatively large.

The use of a relation in the log-law region (for example Equation 2.62) is called high-Reynolds simulation. For high-Reynolds, grading near the wall is often not needed. This makes the calculation much faster, but gives more inaccuracy.

2.7. Hopper Models

In this paragraph, all important hopper models are reviewed. Keeping the processes of Paragraphs 2.2 to 2.6 in mind, it will be discussed to which extend the models represent reality.

2.7.1. Camp

Camp[1] assumed a hopper with a horizontal velocity U, which is constant over the height. Camp does not take the hindered settling effect into account, so each particle moves with a straight line as can be seen in Figure 2.14.

v_0 is called the 'hopper load parameter':

$$v_0 = U\frac{H}{L} = \frac{Q}{WL} \tag{2.70}$$

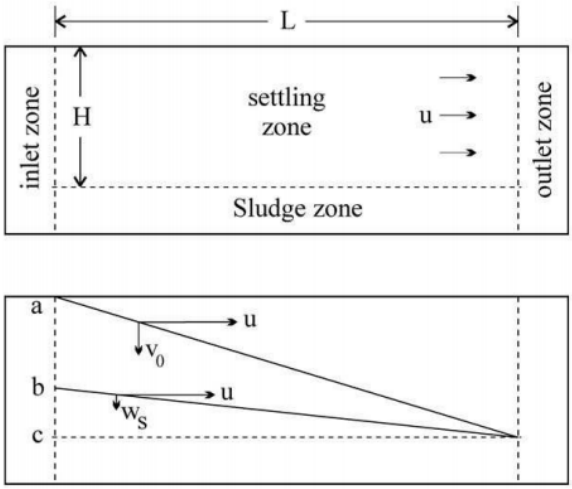

Figure 2.14: Ideal settling basin according to Camp.

The hopper load parameter is the settling velocity needed to travel from 'point a' (Figure 2.14) to the end of the bed. This means that if a particle fraction has a settling velocity which is bigger than the hopper load ($w_s > v_0$), all particles with this particle diameter will reach the bed independent of the height at which these particles enter the hopper. This is the fraction $1 - p_0$ of the PSD (figure 2.15).
The particles with $w_s < v_0$ will only settle depending on the height on which they enter the settling zone (fraction $p_0 - p_s$). After doing some derivation, it can be found that the percentage of these particles which reach the bed is $w_s(p)/v_0$.
The smallest particles (fraction p_s) will not settle, because for these particles the horizontal velocity U exceeds the scour velocity:

$$U_s(D) = \sqrt{\frac{8\,(1-n_0)\,\mu\Delta g D}{f}} \tag{2.71}$$

The removal ratio is the percentage of all particles which settle onto the bed and can be determined by:

$$r_r = 1 - p_0 + \int_{p_s}^{p_0} \frac{w_s(p)}{v_0} dp \tag{2.72}$$

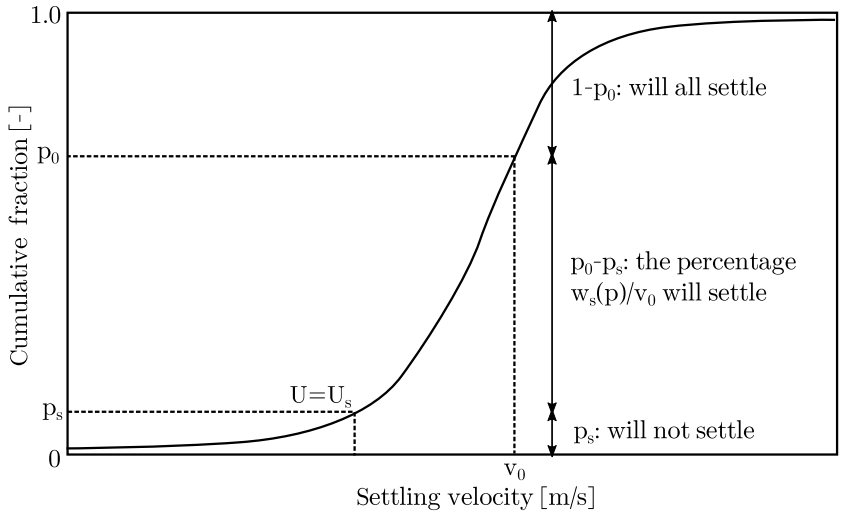

Figure 2.15: Cumulative PSD as function of the settling velocity

Influence of turbulent diffusion
In a later article, which was inspired on the work of Dobbins[3], Camp[2] described the effect of turbulence. By simplifying the advection-diffusion equation (Equation 2.44), Camp arrived at the following equation:

$$U\frac{\partial \alpha}{\partial x} = \Gamma_z \frac{\partial^2 \alpha}{\partial z^2} + w_s \frac{\partial \alpha}{\partial z} \tag{2.73}$$

To arrive at this formula, Camp made the following simplifications:

1. Stationary flow: $\frac{\partial \alpha}{\partial t} = 0$
2. The horizontal velocity U is constant in x- and z-direction. In reality, however, a buoyant jet and density current can be observed.
3. The turbulent diffusion coefficient Γ is constant in x- and z-direction.
4. The vertical mixture velocity is zero, therefore: $w = -w_s$. The hindered settling effect is not taken into account: $w_s \neq f(c)$

An analytical solution of Equation 2.73 was found by separation of variables. Since the analytical solution was cumbersome in usage, Camp presented his results in the form of figure 2.16. For the turbulent diffusion coefficient Camp used $\Gamma_t = 0.075 H u_*$ in which u_* and H are the shear velocity and total height above the bed, respectively. The removal ration can be calculated with:

$$r_r = \int_{p_s}^{1} r_{r,g}(p) \frac{w_s(p)}{v_0} dp \tag{2.74}$$

Next to the assumptions described above to arrive at Equation 2.73, the following assumptions also lead to discrepancy:

1. Pickup cannot be calculated correctly, since the density current is not modelled.
2. The bed doesn't rise or erode.

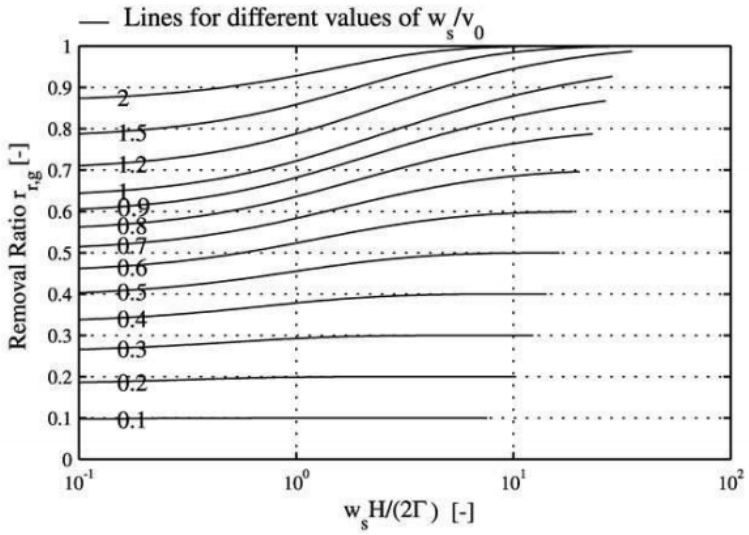

Figure 2.16: Removal rate with the influence of turbulence

3. The time effect: particles which enter the hopper and don't settle are assumed to leave the hopper instantly. In reality particles stay for a while in the hopper. The concentration of the mixture above the bed influences the overflow concentration.

2.7.2. Vlasblom and Miedema

Vlasblom and Miedema[5] also assumed a uniform flow profile. By fitting the curves in Figure 2.16, new explicit equations for $r_{r,g}$ were developed. These formulas are a lot easier to use than the analytical equations of Camp. Over the years Vlasblom and Miedema have been adding features to improve the model of Camp:

1. The rise of the sand bed in their article of 1996[5]
2. Initially, Vlasblom and Miedema used Equation 2.71 to calculate the critical diameter. Later on, they used a method based in Shields[7]. This still gives an underestimation of the erosion. In reality, the velocity at the bottom is higher due to the density current.
3. Ooijens[6] added the time effect by regarding the hopper as an ideal mixing vessel.
4. An estimation of the thickness of the layer of water above the overflow[7]

A clear advantage of the model of Miedema is its simplicity and low calculation times. On the other hand, this simplicity also gives rise to some inaccuracy or effects which are not incorporated:

1. Since the density current at the bottom is not modelled, there cannot be correctly accounted for the scour. The critical diameter is now calculated with a wrong velocity profile.
2. Due to the wrongly assumed velocity pattern, the turbulence may differentiate.
3. The near bed concentration cannot be calculated, so it needs to be estimated.

The model of Miedema can predict the overflow losses quite well as can be seen in 2.17 and 2.22. At the beginning of the loading cycle, though, the overflow concentration is too high and at the end it is too low. This is due to the uniform velocity profile, which has low velocities at the beginning of the cycle and higher velocities towards the end.

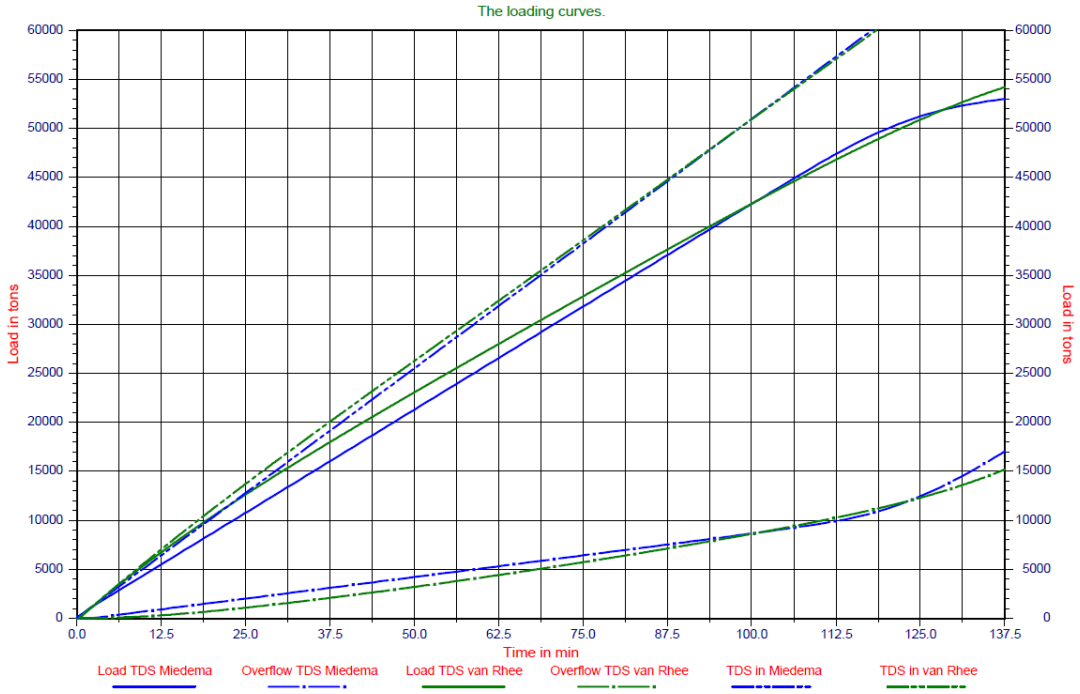

Figure 2.17: Comparison of the models of Van Rhee and Miedema[9]

2.7.3. 1DV Model Van Rhee

Van Rhee models the hopper as in Figure 2.18. In this model, the following simplifications are made:

1. The sand is uniformly distributed over the whole surface of the hopper
2. The inflow concentration and discharge which enter zone 2 are assumed to be the same as at the inflow of the hopper
3. All quantities are assumed to be uniformly distributed over the length of the hopper
4. In reality there is a bed shear stress caused by the density current. This can reduce the sedimentation velocity. With this 1DV model, this effect is not simulated. This is an important simplification as will be seen later on.

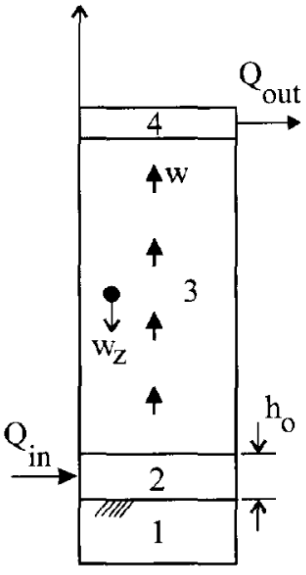

Figure 2.18: 1DV model

The transport of sediment in zone 3 is calculated with the one-dimensional advection-diffusion equation:

$$\frac{\partial \alpha_k}{\partial t} = -\frac{\partial (\alpha_k w_k)}{\partial z} + \frac{\partial}{\partial z}\left(\Gamma_z \frac{\partial \alpha_k}{\partial z}\right) + \delta_{s,k} \tag{2.75}$$

In which $\delta_{s,k}$ is the source term at the inlet and outlet. w_k is the vertical velocity of a certain fraction. Van Rhee derives the following formula for w_k:

$$w_k = w + w_{kr} - \sum_{k=1}^{N} \alpha_k w_{kr} \tag{2.76}$$

w is the bulk velocity which equals Q/A.

w_{kr} is the slip velocity calculated with:

$$w_{kr} = w_{0,k}(1 - \sum \alpha_k)^{n_k - 1} \tag{2.77}$$

For the exponent n_k the relation of Garside is used. Note that $w_{0,k}$ is negative, since a particles moves down during settling.

On model scale, the cumulative overflow losses were predicted well. However, compared to a prototype scale test with the TSHD 'Cornelia', the 1DV model underpredicted the overflow losses by a factor 5. Van Rhee gives an explanation for this. During the model tests, the influence of the bed shear stress on the sedimentation was negligible. At prototype scale, the influence of the bed shear stress has become significant due to scale effects.

2.7.4. 2DV model Van Rhee

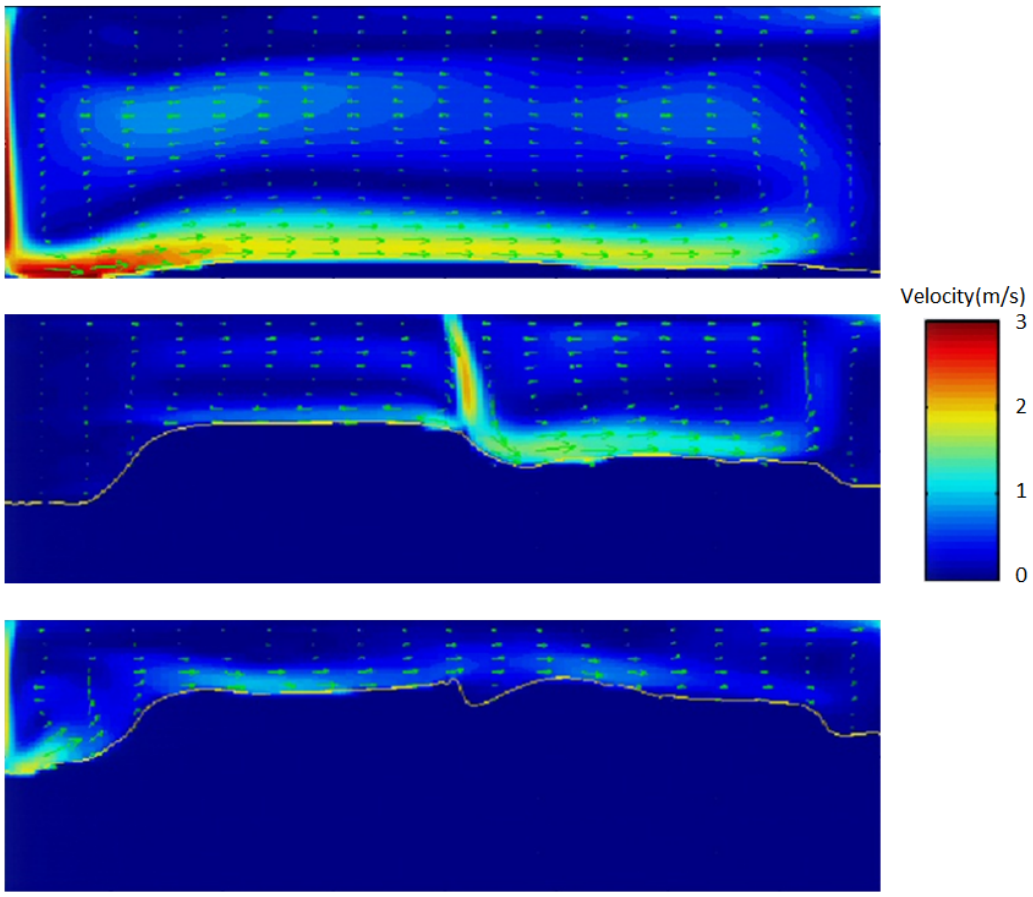

Figure 2.19: Velocities in a hopper at three time steps simulated with the 2DV model of Van Rhee.

Van Rhee also developed a 2D model. An example of a simulation can be seen in Figure 2.19. Comparison between model and measurements show good resemblance. Differences between measured an simulated overflow losses are small. The velocity profiles are similar and show the same behaviour over time. The density current of Figure 2.1 is observed. Also the return flow of Figure 2.2 is computed. The quantitative values are however slightly different. At the inlet, the flow velocity in the jet is higher. This leads the higher entrainment and hence more dilution of the inflowing mixture. The concentration

of the density current above the bed is therefore lower. This higher velocity in the jet is caused by the choice of turbulence model. Air entrainment can also play a role. A large improvement of the model is the calculation of the reduced sedimentation due to the bed shear. The simulations of this model give a lot of insight into the processes inside the hopper.

2.7.5. Spearman

The 1DV model of Spearman[11] looks very similar to the 1DV model of Van Rhee. The hopper is divided in 20 cells which are layered on top of each other. Just like Van Rhee, he assumes that the sediment influx is uniformly distributed over the bottom of the hopper. Also the vertical transport is described with Equations 2.75 and 2.76.

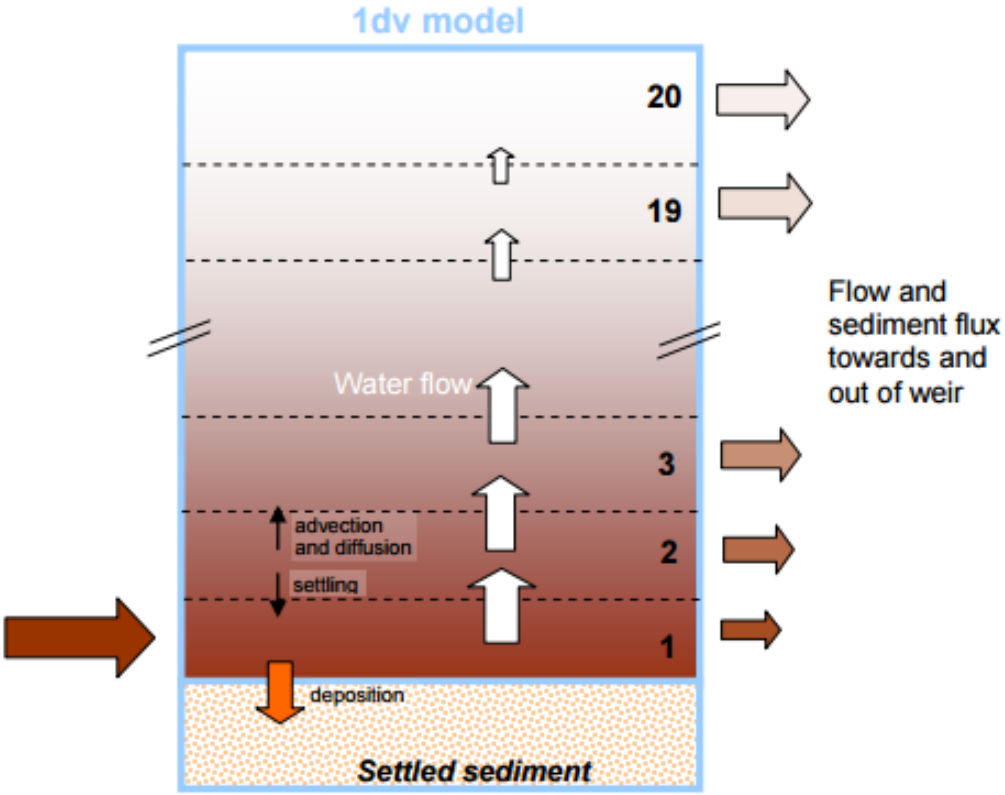

Figure 2.20: 1DV Model of Spearman

The difference between the models is the outflow. In the model of Van Rhee(Figure 2.3b) there is only outflow at the top. Spearman assumes that sediment from every layer flows into the overflow. In his model there is horizontal flow in the whole hopper. When the mixture arrives at the end of the hopper, everything moves up and goes through the overflow.

To calculate the horizontal velocity first the pressure gradient is calculated. Every layer is assumed to have the same value of the pressure gradient:

$$\frac{1}{\rho}\frac{\partial p}{\partial x} = -\frac{\tau_b}{\rho h_{water}} + \frac{U(t) - U_0(t)}{T_{rel}} \tag{2.78}$$

ρ is the water density
τ_b is the shear stress imparted on the bed
h_{water} is the water depth
U is the mean horizontal velocity during the last time-step

U_0 is the desired mean velocity which is $Q/(W * H)$
T_{rel} is the relaxation time. For this value twice the time step is used.

Next, this value is used to compute the velocities with the one-dimensional equation for horizontal momentum:

$$\frac{\partial u}{\partial t} + \frac{1}{\rho}\frac{\partial p}{\partial x} = \frac{\partial}{\partial z}\left((\nu_m + \nu_e)\frac{\partial u}{\partial z}\right) \tag{2.79}$$

ν_m and ν_e are the molecular viscosity and eddy viscosity, respectively. The shape of the velocity profile can be seen in Figure 2.20. With these horizontal velocities, the outflow is calculated.

Since Spearman's model has a horizontal velocity, a bed shear could be calculated. However, Spearman doesn't model the density current causing the erosion to be lower.

The 1DV of Van Rhee was not able to predict overflow losses at prototype scale. On the contrary, comparing the 1DV model of Spearman with measurements of the TSHD the 'Oranje', it was shown that the model is able to predict these overflow losses very well. According to Spearman, at the end of the loading cycle, the density current plunges directly into the overflow causing higher overflow losses. Since sediment from every layer goes into the overflow, the overflow losses for Spearman are higher than the 1DV model of Van Rhee, giving better resemblance at prototype scale.

2.7.6. Braaksma

The model of Braaksma[12] was designed for the field of System & Control. The future goal of this model is controlling a dredger. By using this sedimentation model, the ideal trajectory of the pump settings, drag head settings and sailing speed for the next 5 minutes could be calculated. To calculate the ideal trajectory, the calculation speed is a very important. Braaksma accounts for erosion by using reduced sedimentation:

$$v_{sed} = R(\theta, \alpha_b) v_{sed,0} \tag{2.80}$$

Braaksma calculates $R(\theta, c_b)$ in an alternative way:

$$R = \frac{Q^2}{k_e * h_m^2} \tag{2.81}$$

h_{water} is the height of the water above the bed and k_e a constant defined with a least square method. The increase in bed volume can then be calculated with:

$$Q_s = A v_{sed} = A \cdot R(\theta, \alpha_b) \frac{-\alpha_b w_0 \left(1 - \alpha_b\right)^n}{1 - n_0 - \alpha_b} \tag{2.82}$$

For the near bed concentration the following formula is used:

$$\alpha_b = \frac{\rho_m - \rho_w}{\rho_s - \rho_w} \tag{2.83}$$

The mixture density, ρ_m, he determines by assuming a density profile over the height. For this he tested three options: a linear, an exponential and a two layer model. After validation with measurements on a TSHD, the two layer model appeared to be the best. ρ_m is calculated with the total mass of all the particles in the mixture divided by the mixture volume. ρ_m is assumed to be constant in the layer above the bed. This leads to a near bed concentration which is too low (Equation 2.83).

In the model of Braaksma it is not needed to use a particle diameter as input. During the first dredging cycle on an excavation site the bed height, overflow level, inflow concentration and inflow discharge are measured. Next, the $w_{s,0}$, k_e, ρ_{bed} and n(exponent of hindered settling) are determined with a least squares method. The first loading cycle is modelled with different values of $w_{s,0}$, k_e, ρ_{bed} and n. The values which give the best fit are used in the rest of the loading cycles at that excavation site.

Because Braaksma has the possibility of using a least squares method, a less accurate model can still give reasonable results. In this thesis a least squares method is not possible.

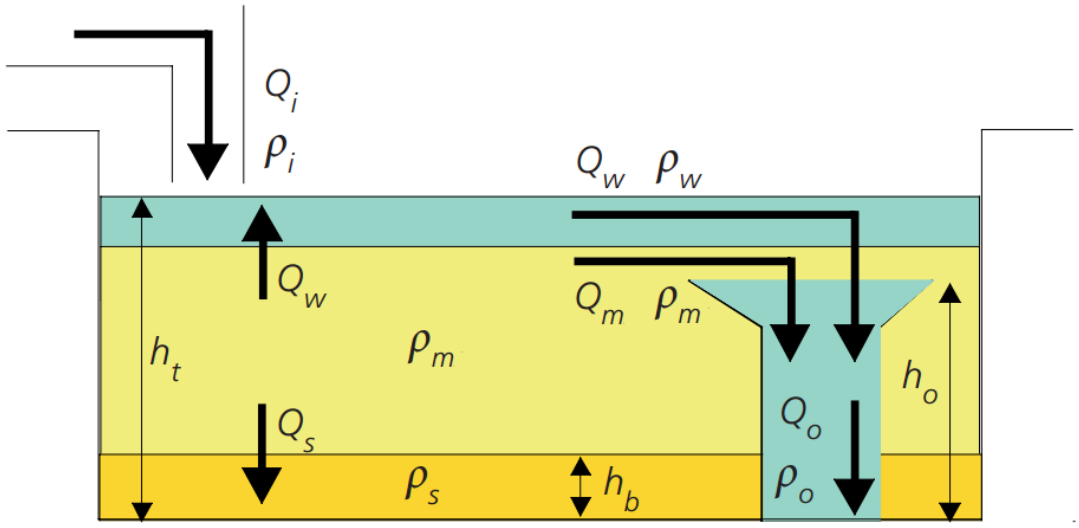

Figure 2.21: Two layer model

2.7.7. Jensen

Jensen inspired his model on Braaksma. An improvement on the model of Braaksma is the usage of a PSD. Contrary to Braaksma, Jensen uses only one mixture layer instead of two. The concentration of every particle diameter is assumed to be constant throughout the whole layer. To calculate the sedimentation velocity he uses a non-dimensional variant of:

$$v_{sed} = \frac{-\sum(\alpha_k w_k)}{1 - n_0 - \sum \alpha_k} \tag{2.84}$$

w_k was calculated with $w_{0,k}(1-\sum \alpha_k)^{n_k}$. This is possible, because perfect mixing is assumed. Normally, w_k should be calculated with Equation 2.76.

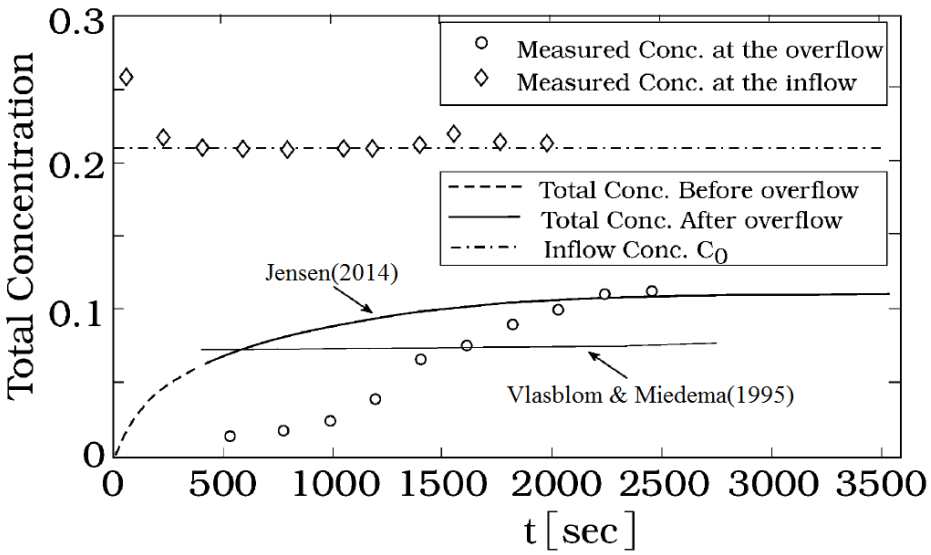

Figure 2.22: Overflow concentration of Test 5 of Van Rhee[10]

The results of this model are poor (Figure 2.22). The concentration of the particles is assumed to be homogeneous, so when the water level reaches the overflow, directly a high concentration of particles leaves the hopper.

2.7.8. Konijn

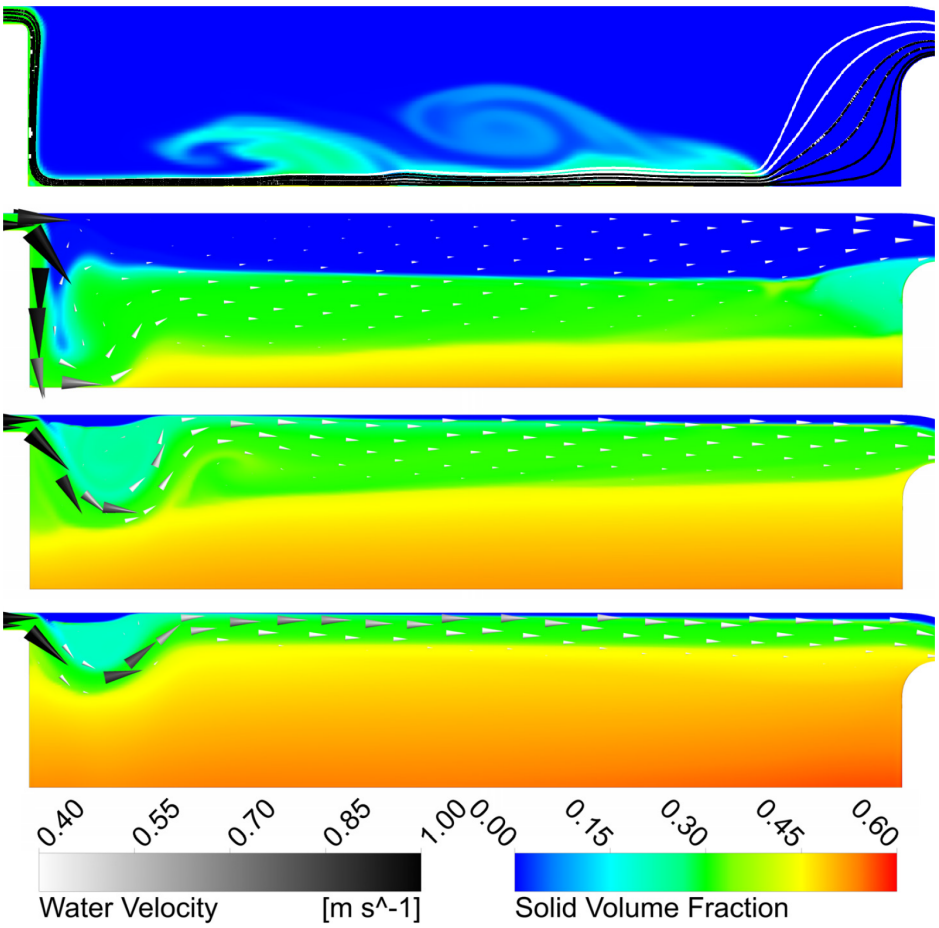

Figure 2.23: Concentration and velocity after 7 s, 39 s, 100 s and 170 s. $d = 200\ \mu m$, $\alpha_i n = 0.3$ and $u_{in} = 1\ m/s$

Konijn[14] has also made a 2DV model. Konijn used an Euler-Euler approach. As explained in Paragraph 2.6.1, a big challenge with Euler Euler is determining the coupling forces. In his model, the coupling forces were causing instabilities, hence calculation times were huge. To make sure the calculation time was days instead of weeks, Konijn used a hopper of 1 by 5 meter(a mesh of 90 x 350). Figure 2.23 is an example of a simulation.

The results of the model are poor. The first thing that can be seen is that there is no (or almost none) entrainment in the inflowing jet. Secondly, the density current disappears very quickly in the model. During Test 8 (Figure 2.1) a density current is present throughout the whole measurement.

Bibliography

[1] Camp T. R. (1936). ”A study of the rational design of settling tanks.” Sewage Works Journal 8(5), pp, 742-758.

[2] Camp, T.R. (1943). ”The effect of turbulence on retarded settling.” Proceedings of the 2nd Hydraulics Conference, University of Iowa, Studies in Engineering, Bulletin 27, pp. 307-317.

[3] Dobbins, W. E.(1943). “The effect of Turbulence on Sedimentation.” Proc. Am. Soc. Civil Engineers, Vol. 69, No. 2, pp. 235-262.

[4] Groot, J. (1981). ”Rapport Beunbezinking”. Papendrecht: Royal Boskalis Westminster.

[5] Miedema, S.A., Vlasblom, W. (1996). ”Theory of Hopper Sedimentation”. 29th Annual Texas A&M Dredging Seminar, New Orleans: WEDA.

[6] Ooijens, S. (1999). ”Adding Dynamics to the Camp Model for the Calculation of Overflow Losses”. Terra et Aqua, 76, pp. 12-21.

[7] Miedema, S. (2008), ”An Analytical Approach To The Sedimentation Process In Trailing Suction Hopper Dredgers”. Terra et Aqua, 112, pp. 15-25.

[8] Miedema, S. (2009). ”The effect of the bed rise velocity on the sedimentation process in hopper dredges”. Journal of Dredging Engineering, Vol. 10, No. 1 , pp. 10-31.

[9] Miedema, S.A., Rhee, C. van (2007) ”A sensitivity analysis on the effects of dimensions and geometry of Trailing Suction Hopper Dredges”. WODCON, Orlando, USA.

[10] Van Rhee, C. (2002). ”On the sedimentation process in a Trailing Suction Hopper Dredger”. PhD thesis, TU Delft, the Netherlands

[11] Spearman, J. (2013) ”TASS Software - User Guide for TASS version 4.0”. HR Wallingford

[12] Braaksma, J., Klaassens, J. B., Babuska R., de Keizer, C.(2007). ”A computationally efficient model for predicting overflow mixture density in a hopper dredger”. Terra et Aqua, 106, pp. 16-25.

[13] Jensen, J.H., Saremi, S.(2014). ”Overflow concentration and sedimentation in hoppers” J. Waterw., Port, Coast. Ocean Eng., ASCE, 40.

[14] Konijn, B.J. (2016). ”Numerical simulation methods for dense-phase dredging flows”. PhD thesis, Universiteit Twente, the Netherlands

[15] Rodi, W. (1993) ”Turbulent Buoyant Jets and Plumes”. Oxford, Pargamon.

[16] Yannopoulos, P. C. (2006). ”An improved integral model for plane and round turbulent buoyant jets”. J. Fluid Mech., 547, 267–296

[17] Kotsovinos, N.E. (1977). ”Plane turbulent buoyant jets. Part 1. Integral properties”. J. Fluid Mech., 81, pp. 25-44.

[18] Ramaprian, B.R., Chandrasekhara, M.S. (1989). ”Measurements in vertical plane turbulent plumes”. J. Fluids Eng., 111, pp. 69–77.

[19] Parker, G., Fukushima, Y., and Pantin, H. M. (1986). ”Self-accelerating turbidity currents”. J. Fluid Mech., 171, pp. 145-181.

[20] Sequeiros, O.E.(2010). ”Characteristics of velocity and excess density profiles of saline underflows and turbidity currents flowing over a mobile bed”. Journal of Hydraulic Engineering, 136, pp. 412–434.

[21] Brennan, D.(2001). ”The numerical simulation of two-phase flows in Settling Tanks”. PhD thesis, Imperial College of Science, Technology and Medicine, Department of Mechanical Engineering, London.

[22] Goeree, J.C., Van Rhee, C., Bugdayci, H.H.(2013). ”Numerical sediment simulation using a continuous flow-model.” Multiphase, 16, pp. 323-335, BHR Group, Bedford, UK.

[23] Goeree, J.C.(2016). ”Concentration and Velocity Profiles of Sediment-Water Mixtures using the Drift Flux Model” The Canadian Journal of Chemical Engineering, 94, pp. 1048-1058.

[24] Chieng, C. C., Launder, B. E. (1980). ”On the Calculation of Turbulent Heat Transport Downstream From an Abrupt Pipe Expansion.” Numerical Heat Transfer, 3, pp. 189-207

[25] Patel, V. P., Rodi, W., Scheuerer, G. (1985). ”Turbulence Models for Near-Wall and Low Reynolds Number Flows: A Review.” AIAA Journal, 23, pp. 1308-1319

[26] Cebeci, T., Smith, A. M. 0. (1974). Analysis of Turbulent Boundary Layers. New York: Academic Press

[27] Celik, I.B.(1999). ”Introductory turbulence modeling”. Lecture Notes, West Virginia University.

[28] Han, Z., Reitz, Z.D.(1995). ”Turbulence modeling of internal combustion engines using RNG $k-\epsilon$ models” Comb. Sci. Tech. 106, 267 (1995).

[29] Shih, T.H., Liou, W. W. Shabbir, A., Yang, Z. and Zhu, J.(1994). ”A New k–e Eddy Viscosity Model for High Reynolds Number Turbulent Flows—Model Development and Validation”. NASA TM-106721.

[30] Van Rijn, L. C. (1984). ”Sediment pick-up functions”. Journal of Hydraulic Engineering, 110(10), pp.1494–1502.

[31] Brownlie, W. R., Brooks, N. H. (1981). ”Compilation of alluvial channel data: laboratory and field”. WM Keck Laboratory of Hydraulics and Water Resources, California Institute of Technology Pasadena, CA.

[32] Van Rhee, C., Talmon, A. (2010). ”Sedimentation and erosion of sediment at high solids concentration”. Proceedings of Hydrotransport 18, pp. 211-222, BHR Group, Bedford, UK.

[33] Van Rhee, C. (2015). ”Slope failure by unstable breaching”. Maritime Engineering, 184, pp. 84-92

[34] Blocken, B. (2007) ”Cfd simulation of the atmospheric boundary layer: wall function problems.” Atmospheric Environment, 41, pp. 238-252.

[35] Brouwers, J.J.H. (2007) ”Dissipation equals production in the log layer of wall-induced turbulence.” Physics of fluids, 19

[36] Cheng , N. S.(1997). ”Simplified settling velocity formula for sediment particle”. Journal of Hydraulic Engineering, American Society of Civil Engineers, v. 123, pp. 149-152.

[37] Ferguson, R., Church, M.(2004). ”A Simple Universal Equation for Grain Settling Velocity”. Journal of Sedimentary Research, vol. 74, n. 6, pp. 933–937

[38] Richardson, J. and Zaki, W. (1954). ”Sedimentation and Fluidisation: Part I”. Transactions of the Institution of Chemical Engineers, 32, pp. 35-53

[39] Garside, J., Al-Dibouni, M.R. (197). ”Velocity-Voidage Relationships for Fluidization and Sedimentation in Solid-Liquid Systems” Ind. Eng. Chem., Process Des. Dev., Vol. 16, No. 2, pp. 206-214.

[40] Baldock, T.E.(2003). ”Settling velocity of sediments at high concentrations”. Coast. Eng., 51, pp. 91-100

[41] Pal, D., Ghoshal, K. (2013) ”Hindered settling with an apparent particle diameter concept”. Advances in Water Resources, 60, pp. 178–187.

[42] Choi, S., García, M. H. (2002). "k–ϵ turbulence modeling of density currents developing two dimensionally on a slope." J. Hydraul. Eng., 128(1), pp. 55–63.

[43] Sobera, M., Kleijn, C.(2008) "T-RANS Simulations of Subcritical Flow with Heat Transfer Past a Circular Cylinder Surrounded by a Thin Porous Layer," Journal of Flow, Turbulence and Combustion 80 (4), pp. 531-546.

[44] Yakhot, V., Orszag, S.A.(1986). "Renormalization group analysis of turbulence. 1. Basic theory." J. Sci. Comput., 1(1), pp. 3–51.

[45] Menter, F.R.(1992). "Influence of freestream values on k-ω turbulence model predictions." AIAA Journal, Vol. 30, No. 6.

A

RANS models

In Paragraph 2.6.4 the idea behind turbulence modelling was explained. In `OpenFOAM`, several RANS models are available. A discussion about the different models is given in this appendix.

Standard k-ϵ model
In a k-ϵ model the turbulent eddy viscosity is calculated with:

$$\nu_e = c_\mu \frac{k^2}{\epsilon} \tag{A.1}$$

The k is the turbulent energy and ϵ is the dissipation of turbulent energy. Both are calculated with their own transport equation.

$$\frac{\partial k}{\partial t} + \frac{\partial (uk)}{\partial x} + \frac{\partial (wk)}{\partial z} = \frac{\partial}{\partial x}\left(\frac{\nu_e}{\sigma_k}\frac{\partial k}{\partial x}\right) + \frac{\partial}{\partial z}\left(\frac{\nu_e}{\sigma_k}\frac{\partial k}{\partial z}\right) + P + P_b - \epsilon \tag{A.2}$$

$$\frac{\partial \epsilon}{\partial t} + \frac{\partial (u\epsilon)}{\partial x} + \frac{\partial (\epsilon k)}{\partial z} = \frac{\partial}{\partial x}\left(\frac{\nu_e}{\sigma_\epsilon}\frac{\partial \epsilon}{\partial x}\right) + \frac{\partial}{\partial z}\left(\frac{\nu_e}{\sigma_\epsilon}\frac{\partial \epsilon}{\partial z}\right) + c_{1\epsilon}\frac{\epsilon}{k}P + c_{1\epsilon}c_{3\epsilon}\frac{\epsilon}{k}P_b - c_{2\epsilon}\frac{\epsilon^2}{k} \tag{A.3}$$

The coefficients can for example be found in Celik[27]. The k-ϵ model has certain advantages and disadvantages. It has a good convergence rate and relatively low memory requirements. The biggest disadvantages are inaccuracy with adverse pressure gradients, strong curvature to the flow.

During the validation of his model, Van Rhee[10] also encountered problems with jets. For neutrally buoyant jets the spreading is too small. This resulted in velocities which were too high. For buoyant jets, the spreading is even less than for the neutrally buoyant jets. It is unclear if this was caused by the k-ϵ model or the settings during the simulations.

`OpenFOAM` has two versions of the standard k- model: `kEpsilon` and `buoyantKEpsilon`. In `kEpsilon` the buoyancy term P_b is omitted. In this thesis, `buoyantKEpsilon` is used.

By default, in $c_{3\epsilon}$ is one in `buoyantKEpsilon`. Inspired by the work of Henkes[**?**], $c_{3\epsilon}$ is also multiplied by a factor $\tanh(v/u)$ in `buoyantKEpsilon`. This means that in horizontal flow $c_{3\epsilon}$ is zero and in vertical flow $c_{3\epsilon}$ is one.
Choi & Garcia[42] gave an overview of different researches about the $c_{3\epsilon}$. For vertical flow, $c_{3\epsilon}$ should indeed be one. For horizontal flow, experiments show mixed results. For stably stratified flows, $c_{3\epsilon}$ varies between zero and 0.5. For unstable horizontal flows, $c_{3\epsilon}$ can be expected to be one.
In figure A.1, it can be seen that $c_{3\epsilon}$ has some influence. A low $c_{3\epsilon}$ causes more stratification. In this thesis, the $\tanh(v/u)$-term is omitted. If that is a good choice can be questioned. Keeping the overview of Choi in mind, a term of $0.3 + 0.7\tanh(v/u)$ would probably be better. Some more research is advisable.

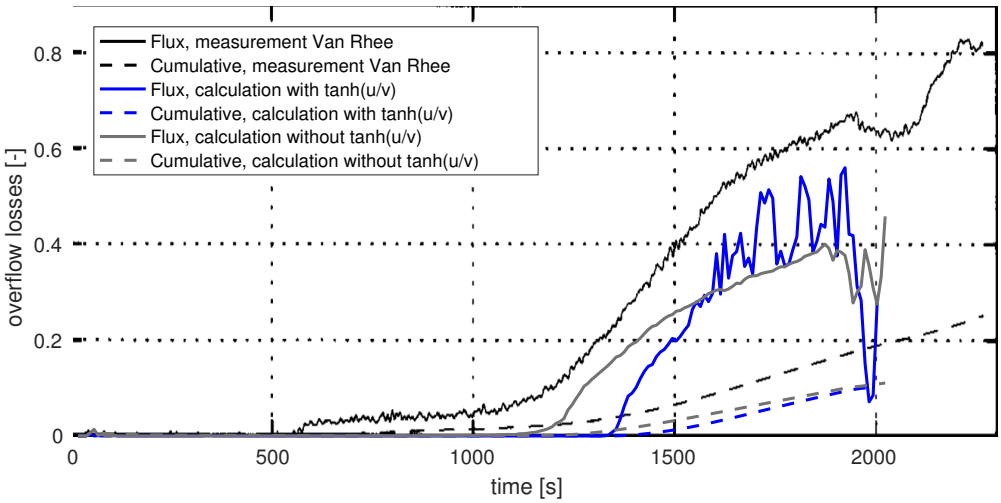

Figure A.1: Influence of $c_{3\epsilon}$ on the overflow losses of Test 8. An inlet of 8 cm, which is rather big, and a very fine mesh was used. The flux is defined as $\frac{\alpha_{out}(t)Q_{out}(t)}{\alpha_{in}(t)Q_{in}(t)}$.

RNG-k-ϵ model

The RNG-k-ϵ model is derived from the instantaneous Navier–Stokes equations by using a mathematical technique called renormalization group theory[43][44]. It has a correction that reduces the modeled turbulence in presence of large vortical structures. Therefore, it has improved accuracy in rotating flows.

One of the differences with the standard k-ϵ model is a varying $c_{2\epsilon}$:

$$c_{2\epsilon}^{*} = c_{2\epsilon} - \frac{\eta\left(1 - \frac{\eta}{\eta_0}\right)}{1 + \gamma\eta^3} \tag{A.4}$$

Where γ=0.012 and η_0=4.38.

$$\eta = \sqrt{\frac{P}{c_\mu \epsilon}} \tag{A.5}$$

The rest of the coefficients differ only slightly from the standard $k - \epsilon$ model and can for example be found in Han[28] or Van Rhee[10]. Van Rhee[10] did several tests with the RNG-k-ϵ model. In some situations it resulted in improvements, but sometimes the results became worse.

Realizable-k-ϵ model

The realizable-k-ϵ model is another variation on the standard k-ϵ model. The main difference is the calculation of c_μ:

$$c_\mu = \frac{1}{A_0 + A_s \frac{kU^*}{\epsilon}} \tag{A.6}$$

For the determination of A_s, A_0, U^* and the other variables the reader is referred to Shih[29]. Also the transport equations of k and ϵ are different than in the standard k-ϵ model. Shih validated the realizable model for jets. The spreading rate with the realizable model is closer to measurement results the standard k-ϵ model.

k-ω model

In the k-ω model the eddy viscosity is calculated by:

$$\nu_e = \frac{k}{\omega} \tag{A.7}$$

Both the kinetic energy k and The specific dissipation rate ω are calculated with their respective transport equation. The k-ω model is more accurate than k-ϵ near the wall. Therefore, it performs significantly better for adverse pressure gradients and separation. In the freestream outside the boundary

layer, k-ϵ gives better performance since the ω-equation shows a strong sensitivity in this region[45]. In addition, the need of high mesh resolution near the wall causes extra calculation time.

SST-k-ω model
The SST-k-ω model is a combination of k-ω and k-ϵ. k-ω is used near the wall and k-ϵ is used in the rest of the domain. This also leads to more calculation time. Just like the standard k-ω model, it is too much effort to implement this model in `driftFluxFoam`.

B

Derivation Boundary Conditions

In the log-layer, the dissipation of turbulent kinematic energy equals the production[35]:

$$\rho\epsilon = P \tag{B.1}$$

$$\rho\epsilon = \tau\frac{\partial u}{\partial y} \tag{B.2}$$

$$\rho\epsilon = \rho u_*^2\frac{\partial u}{\partial y} \tag{B.3}$$

$\frac{\partial u}{\partial y}$ can be calculated by taking the derivative of equation 2.62 or 2.69. This both leads to:

$$\frac{\partial u}{\partial y} = \frac{u_*}{\kappa y} \tag{B.4}$$

Equation B.4 can be substituted in equation B.3:

$$\epsilon = \frac{u_*^3}{\kappa y} \tag{B.5}$$

Equation B.1 can also be used to derive an equation for k:

$$\rho\epsilon = P \tag{B.6}$$

$$\rho\epsilon = \tau\frac{\partial u}{\partial y} \tag{B.7}$$

The shear stress can be calculated with:

$$\tau_e = \mu_e\frac{\partial u}{\partial y} = C_\mu\frac{k^2}{\epsilon}\frac{\partial u}{\partial y} \tag{B.8}$$

Substitution in equation B.7 leads to:

$$\rho\epsilon = \rho C_\mu\frac{k^2}{\epsilon}\frac{\partial u}{\partial y}\frac{\partial u}{\partial y} \tag{B.9}$$

Substitution of equation B.4 leads to:

$$\epsilon^2 = C_\mu k^2 \frac{u_*^2}{\kappa^2 y^2} \tag{B.10}$$

By using B.5 we get:

$$\frac{u_*^6}{\kappa^2 y^2} = C_\mu k^2 \frac{u_*^2}{\kappa^2 y^2} \tag{B.11}$$

$$k = \frac{u_*^2}{C_\mu^{0.5}} \tag{B.12}$$

The equations B.5 and B.12 can often be found in literature and are the basis of a lot of CFD-calculations. Van Rhee[10], for instance, uses these equations.

In `OpenFOAM`, the usage of wall functions is slightly different. Since equations B.5 and B.12 can give instabilities, `OpenFOAM` uses a method which is more stable.
During a high-Reynolds calculation, the boundary condition for the k is the `kqRWallFunction`, which is a simple wrapper around the zero-gradient condition. For a high-Reynolds calculation of ϵ the `epsilonWallFunction` is frequently used. To get the `epsilonWallFunction`, equation B.12 needs to be substituted into equation B.5:

$$\epsilon = \frac{C_\mu^{0.75} k^{1.5}}{\kappa y} \tag{B.13}$$

To calculate the k correctly at the first grid-cell, the production of turbulent kinetic energy, P, needs to be calculated correctly. `epsilonWallFunction` therefore does a correction for the production. This seems very easy, because in the log-layer the production equals the dissipation (calculated with equation B.13). `OpenFOAM` does something different, though:

$$P = \tau \frac{\partial u}{\partial y} = \mu_{eff} \frac{\partial u}{\partial y} \frac{\partial u}{\partial y} \tag{B.14}$$

$$P = \mu_{eff} \frac{\partial u}{\partial y} \frac{u_*}{\kappa y} \tag{B.15}$$

In which $\mu_{eff} = \mu_e + \mu_{mixture}$ and μ_e is the turbulent eddy viscosity and $\mu_{mixture}$ is the viscosity of the fluid. Interestingly, only the eddy viscosity is sometimes taken into account to calculate the production of turbulent energy (for example in B.8). In other instances, both the fluid viscosity and eddy viscosity are taken into account (equation B.3 and B.14). Equation B.12 can be substituted for u_*:

$$P = \mu_{eff} \frac{\partial u}{\partial y} \frac{k^{0.5} C_\mu^{0.25}}{\kappa y} \tag{B.16}$$

To calculate the velocity in the first grid-cell, the viscosity at the wall needs to be calculated correctly. These corrections are done in the boundary conditions for the viscosity. All these boundary conditions rely on the following principle:

$$\tau = \mu_{wall} \frac{\partial u}{\partial y} \tag{B.17}$$

$$\rho_w u_*^2 = \mu_{wall} \frac{u}{y} \tag{B.18}$$

$$\rho_w u_*^2 = \mu_{wall} \frac{u}{y} \tag{B.19}$$

$$\mu_{wall} = \frac{\rho_c y u_*^2}{u} \tag{B.20}$$

Now, a smooth or rough wall function can be used to get a formulation of μ_{wall}. For a smooth wall, equation 2.62 is for example used:

$$\mu_{wall} = \frac{\rho_w \kappa y u_*}{\ln(E y_+)} = \frac{\mu_w \kappa y_+}{\ln(E y_+)} \tag{B.21}$$

$$\nu_{eff} = \frac{\nu_w \kappa y_+}{\ln(E y_+)} \tag{B.22}$$

In this thesis the `nutkRoughWallFunction` is used. The `nutkRoughWallFunction` uses equation B.22, but then divides E by a factor $1 + Ck_s^+$ just like in formula 2.68. This factor $1 + Ck_s^+$ accounts for the roughness.